Aquarius Services Corp.
17 Pokahoe Drive
Sleepy Hollow, NY 10591
USA

Phone: +1 (914) 366-8875
Fax: +1 (914) 366-8876
e-mail: Stras69@worldnet.att.net

Advanced Nuclear Technology
Uppsala Science Park
SE-751 83, Uppsala
SWEDEN

Phone: +46-(0) 18-50 66 80
Fax: +46-(0) 18-50 66 85
e-mail: Ant@ant.se

ZIRAT SPECIAL TOPICAL REPORT ON MANUFACTURING

Peter Rudling and Ronald B. Adamson

Contents

1 INTRODUCTION

This special topical report on zirconium alloy manufacturing and impact on in-pile fuel performance has been prepared within the ZIRAT-5 program.

The objective of this report is to provide members with the basic understanding of the mechanisms involved and their relationship to fuel performance. The report covers the range from basic information to current knowledge and is written and explained in such a way that engineers and researchers not familiar with the topic can easily follow the report, and can find and grasp the appropriate information. This means that the report could be used by the organisation in the training of their internal staff.

The zirconium material performance in-reactor depends on the reactor environment (water chemistry, fast flux, fast fluence, power history, temperature, etc.) and the material itself that in turn is a function of the material chemistry and microstructure. The material microstructure is a function of chemistry and manufacturing history. There are numerous cases reported in the literature when a non-optimised manufacturing process resulted in material problems such as, for instance, excessive corrosion. Thus, a better knowledge of the impact of the manufacturing process on the in-reactor material performance may reduce the risk of unexpected surprises for example when a fuel vendor changes its manufacturing process.

More specifically the following topics are covered in the report:

Sponge manufacturing

Ingot melting

Tube (liner, non-liner, duplex), plate and sheet Zircaloy manufacturing

CANDU Zr2.5Nb pressure tube manufacturing

Russian alloy manufacturing (Alloys E110, E635)

Plastic deformation such as forging, rolling, pilgering

Heat treatments such as beta-quenching, recrystallization and stress relieve annealing

Phase transformations solubilities, and the formation of intermetallic compounds

Fundamentals on crystallography, texture, and anisotropy

Plastic deformation, including discussion of deformation systems, dislocation glide, twinning, and dislocation climb

Development of texture, characterisation of texture (pole figures, …)

Welding (TIG, electron beam, laser, plasma, resistance)

Impact of Zirconium processing and chemistry on microstructure, such as texture and second phase particle characteristics (size distribution and chemical composition), dislocation density, and chemical composition homogeneity and their effect on in-pile performance will be discussed throughout the report

Quality control parameters that are particularly important to control for reliable fuel performance will be emphasised

Influence of fabrication on in-reactor performance

2 DEVELOPMENT OF ZIRCONIUM ALLOYS

The Swedish chemist Berzelius succeeded in 1824 to produce impure zirconium powder by reduction of potassium zirconium fluoride with sodium. In 1865 Troost was able to produce impure metal by reducing gaseous zirconium tetrachloride with magnesium. It was not until in 1925 that Van Arkel, DeBoar and Fast did succeed in developing the first practical method for producing ductile zirconium. Their method was based upon an iodine process in which zirconium iodide decomposes on a hot filament. However, this method is very expensive and it would not be possible to produce large quantities of zirconium with this method. This material is called "crystal bar or iodide Zr".

In the second part of the 1940's, Dr. Kroll succeeded in developing a more economical process at Albany, Oregon, for production of ductile zirconium by reduction of zirconium tetrachloride with molten magnesium in an inert atmosphere. This material is called "sponge Zr".

2.1 DEVELOPMENT OF ZIRCALOY

The development of the Zircaloys were reviewed by Kass, 1962, *Ref.2*, that is summarised in this section.

Systematic testing and research by the US Naval Reactors Branch and the Pittsburgh Naval Reactors office of the U.S. Atomic Energy Commission resulted in:

the development of an efficient hafnium separation process to improve the material neutron efficiency, and different Zircaloys.

This early Zircaloy development work was performed in the laboratories of the U.S. Bureau of mines Albany, Oregon, Argonne National Laboratory, the Metallurgical Laboratory of the Massachusetts Institute of Technology, Battelle Memorial Institute, Iowa State College, Oak Ridge National Laboratory and the Bettis Atomic Power Laboratory of the Westinghouse Electric Corporation.

Tests showed a great variability of the quality of crystal bars from lot to lot and gave additional impetus towards the development of zirconium-base alloys. It was specifically found that the impurity content of crystal-bar zirconium had a very marked effect upon its corrosion resistance to hot water. Samples containing more than 0.004% nitrogen* exhibited rapid corrosion rates within very short time in 680 $^{\circ}$ F water. Additional aims in alloying were to make it possible to employ the less expensive Kroll sponge zirconium process than that of the iodide process material as well as to obtain mechanical property improvements.

Compositions are given in weight percent except where specifically noted.

2.1.1 Zry-1

It was soon discovered independently by Battelle Memorial Institute and Iowa State College that the addition of tin to “impure” zirconium tended to overcome the deleterious effects of nitrogen and to lesser extent, that of carbon and aluminium. The amount of tin necessary to obtain optimum corrosion resistance to “impure” zirconium was found to be dependent upon the nitrogen content of the alloy. Estimations for the nitrogen tolerance limits were made by workers at Massachusetts Institute of Technology and it was recommended that an alloy, containing 2.5% tin that could counteract about 700 ppm nitrogen, be studied. This alloy—sponge zirconium plus 2.5% tin – was later known as Zircaloy-1.

2.1.2 Zry-2, Zry-3, Zry-4

Through an accidental contamination of a zirconium ingot by stainless steel it was realised that the impurities of Fe, Ni and Cr in zirconium drastically improved its corrosion performance, and the alloy development program was extended to evaluate the roles of these elements upon the corrosion characteristics of zirconium. Further investigations of the nitrogen tolerance of zirconium-tin ternary alloys with iron, nickel or chromium showed that the tolerance limits for the ternary alloys were higher than that for the binary zirconium-tin alloys. Concurrently, the Albany Station for the U.S. Bureau of Mines had made a number of refinements to the Kroll process for the preparation of sponge zirconium that yielded a product of lowered nitrogen content. The above information coupled with the knowledge that the corrosion rates of zirconium-tin alloys decrease with decreasing tin content lead to investigation into the properties of zirconium-1.8% tin alloys containing additions of iron, nickel or chromium that subsequently lead to Zry-2, -3 and -4.

2.1.2.1 Zry-2

The composition of early Zircaloy-2 was fixed as follows:

Tin content – 1.5%

Since Zircaloy-1 proved to be unsatisfactory in regard to corrosion resistance, the tin content was dropped to 1.5% from 2.5%. The amount of tin in this early variant of Zircaly-2 was sufficient to neutralise the effect of about 1000 ppm of nitrogen, which was considerably more than would be expected in zirconium sponge material at that time.

Iron content – 0.12%

Data from Westinghouse, Bureau of Mines and M.I.T. indicated that small quantities of iron increased the corrosion resistance in zirconium. An optimum value of 0.22% Fe was indicted from binary alloy studies, but since Zircaloy-2 contained other beneficial elements and it was felt that the total alloy content should be kept to minimum to insure ease in fabrication, the iron content was fixed at 0.12%

Chromium content – 0.1%

The chromium content of Zircaloy-2 was 0.1%. It had been found that chromium was beneficial in preventing corrosion of zirconium. Although data on binary zirconium-chromium alloys indicated that corrosion resistance of zirconium increased with increased chromium content, the amount of chromium was kept at 0.1% so that the hardness of the alloy would not be increased excessively.

Nickel content – 0.05%

Nickel was also shown to increase the corrosion resistance of zirconium, exhibiting its greatest influence of extending the life of zirconium alloys in high temperature steam. An optimum value was 0.25% Ni for binary zirconium-nickel alloys. Since Zircaloy-2 contained other beneficial elements and since total alloy content had to be kept at a minimum to insure easy fabricability, the nickel content was fixed at 0.05%

The first important single property of Zircaloy-2 was its excellent corrosion resistance in high temperature water, in which respect it was vastly superior to that of unalloyed zirconium.

2.1.2.2 Zry-3

In the spring of 1953 a new development program was undertaken to develop new zirconium alloys having corrosion resistance superior to that of Zircaloy-2. This new program, which culminated in the alloy “Zircaloy-3”, was not dictated by any, at that time, know serious deficiency in the properties of Zircaloy-2, but by the desire to improve the alloy. The alloy compositions and designations were as follows:

Zircaloy-3A 0.25% tin, 0.25% iron

Zircaloy-3B 0.50% tin, 0.40%iron

Zircaloy-3C 0.50%, tin, 0.20% iron, 0.20% nickel

Concern over the corrosion resistance of Zircaloy-3 first occurred in the fall of 1956 when test results were obtained from the first lot of commercially produced ingots. The trouble with Zircaloy-3 manifested itself in the form of white corrosion product occurring in local areas strung out in the rolling direction (stringers). Subsequent examination of Zircaloy-2 strip products fabricated in the same technique as the Zircaloy-3 strip products showed the presence of faint grey-white stringers. The principal difference was that the Zircaloy-2 stringers were considerably smaller in size and more uniformly distributed. Further experimental work showed that the mechanism of stringer formation in the two alloys were different. For Zircaloy-3, the stringers were caused by segregated grain boundary precipitates while the stringers in Zircaloy-2 were found to be related to gas voids formed in the metal during inert atmosphere melting. Subsequent experiments showed that vacuum arc-melting techniques greatly minimised the occurrence of stringers in Zircaloy-2. Furthermore, beta quenching proved to be an effective remedial treatment for minimising the stringer effect in Zircaloy-3.

Since Zircaloys –2 and –3 exhibited similar water corrosion properties and the remedial measures for minimising the occurrence of stringers in Zircaloy-2 were easier to apply (vacuum melting), the application of Zircaloy-3 was minimal.

2.1.2.3 Zry-4

Concurrently with the development of Zry-3, it was demonstrated in both out-of-pile and in-reactor experiments that the hydrogen absorption of zirconium alloys was enhance when nickel was present in the alloy. In view of the above observations, it was considered prudent to initiate programs to re-evaluate the Zircaloy-2 compositions, especially in respect to the nickel content and to determine the effect of coolant chemistry upon the hydriding of zirconium.

The results of the program, re-evaluating the Zircaloy-2 composition, resulted in two modifications of Zircaloy-2 – nickel-free Zircaloy-2 and Zircaloy-4. The first alloy, nickel-free Zircaloy-2 is essentially Zircaloy-2 without the nickel addition. The second alloy, Zircaloy-4, contained the same chromium and tin levels as Zircaloy-2 but the iron content was increased to compensate for the removal of nickel.

It was, however, found that nickel-free Zircaloy-2 exhibited poor corrosion resistance at elevated temperatures in steam. Thus it was anticipated that the removal of nickel would result in decreased high temperature steam corrosion resistance. This was verified in 800 and 850 ^{o}F steam tests where nickel-free Zircaloy-2 samples completely disintegrated within short periods of time, while Zircaloys –2 and –4 showed similar good corrosion properties.

Additional results showed that nickel-free Zircaloy-2 consistently picked up less hydrogen in both water and steam than that of Zircaloy-2, while Zircaloy-4 showed lower hydrogen absorption only in water.

2.2 DEVELOPMENT OF ZR-NB ALLOYS

In the former Soviet Union similar alloy development, as described in section 2.1, to obtain a corrosion resistant material with enhanced mechanical strength resulted in Zr-Nb alloys subsequently also used in Canada as pressure tubes in CANDU reactors.

During the last decade, it has however become apparent that the corrosion and hydriding properties of the Zircaloy-4 material for heavy corrosion duty PWR applications are not adequate. Therefore, PWR vendors are today looking into other alloys replacing Zry-4 specifically in high corrosion duty plants. Since it has been shown that Zr-Nb alloys have superior corrosion performance compared to that of Zry-4, in a PWR like environment, most PWR fuel vendors are developing Zr-Nb alloys such as ZIRLO and M5. Most of these Zr-Nb alloys are based upon the Russian alloys, e.g., M5 is a development from the Russian alloy E110 and ZIRLO is a modification of the corresponding alloy E635.

2.3 ASTM SPECIFICATION OF ZIRCONIUM ALLOYS

Even though a large number of different zirconium alloys exist on the market today, only four zirconium alloys are currently listed in the ASTM standards, *Table 2-1*.

Table 2-1: Composition range of standard Zr alloys, Lemaignan and Motta, 1994, Ref.1.

ASTM Ref.	R 60802	R 60804	R 60901	R 60904
Common name	Zircaloy-2	Zircaloy-4	Zr-Nb	Zr-Nb
Alloying elements (mass %)				
Sn	1.2 –1.7	1.2 –1.7	–	–
Fe	0.07–0.2	0.18–0.24	–	–
Cr	0.05–0.15	0.07–0.13	–	–
Ni	0.03–0.08	–	–	–
Nb	–	–	2.4 –2.8	2.5–2.8
O	to be specified on order usually 1000–1400 ppm		0.09–0.13	TBS
Impurities (max. ppm)				
Al	75	75	75	75
B	0.5	0.5	0.5	0.5
Cd	0.5	0.5	0.5	0.5
C	270	270	270	150
Cr	–	–	200	100
Co	20	20	20	20
Cu	50	50	50	50
Hf	100	100	100	50
H	25	25	25	25
Fe	–	–	1500	650
Mg	20	20	20	20
Mn	50	50	50	50
Mo	50	50	50	50
Ni	–	70	70	35
Ni	80	80	80	65
Pb	–	–	–	50
Si	120	120	120	120
Sn	–	–	50	100
Ta	–	–	–	100
Ti	50	50	50	50
U	3.5	3.5	3.5	3.5
V	–	–	–	50
W	100	100	100	100

3 BASIC PROPERTIES OF ZIRCONIUM

3.1 CRYSTALLOGRAPHY

Pure zirconium has an hexagonal closed packed, h.c.p., structure with a *c/a* ratio of 1.593, i.e., a slightly lower ratio than that of the ideal ratio of 1.633. The lattice parameters are a_0 = 0.323 and c_0=0.515 nm, *Douglass, 1971, Ref.3*. At 875°C, Zr undergoes an allotropic phase transformation from the low temperature h.c.p. α phase to the body centred cubic, b.c.c., β phase. On cooling, the phase transformation is either martensitic or bainitic, depending on the cooling rate, with a specific orientation relationship between the new α platelets on the old β grains as follows, *Lemaignan and Motta, 1994, Ref. 1*:

$$(0001)_\alpha \| \{110\}_\beta \quad and \quad \langle 11\bar{2}0\rangle_\alpha \| \langle 111\rangle_\beta$$

3.2 PHYSICAL PROPERTIES

The basic physical properties of zirconium are provided in Table 3-1.

Table 3-1: Major physical properties of Zr, Lemaignan and Motta, 1994, Ref.1.

	Unit	Average	[11$\bar{2}$0] dir.	[0001] dir.
Specific mass	$kg \cdot m^{-3}$	6500		
Thermal expansion	K^{-1}	6.70×10^{-6}	5.20×10^{-6}	1.04×10^{-5}
Young's modulus	GPa		99	125
Lattice parameter	nm		$a_0 = 0.323$	$c_0 = 0.515$
Thermal conductivity	$W \cdot m^{-1} K^{-1}$	22		
Specific heat	$J \cdot kg^{-1} K^{-1}$	276		
Thermal neutron capture cross section	barn	0.185		

The melting point of pure zirconium is 1860°C. The main reasons for choosing zirconium alloys for nuclear application are: 1) its low thermal neutron capture cross section being about 30 times lower than that of iron, 2) its good corrosion/oxidation and mechanical properties at operating and accident conditions.

Being a h.c.p. metal, zirconium has strongly anisotropic properties. The differences in thermal expansion and Young's modulus along the main directions of the h.c.p. crystal induce internal stresses after any heat treatment due to grain-to grain thermal strain incompatibilities, *Lemaignan and Motta, 1994, Ref. 1*. After annealing at 500°C, the <*c*>-planes will consequently be in tension at stresses up to 85 MPa depending on the initial texture, *MacEwen et al,1983, Ref. 4*.

3.3 DIFFUSION DATA

Diffusion data in α-Zr are provided in Figure 3-1. Three main parameters impact diffusivity in α-Zr and α-Zr-based alloys: 1) atomic size of the diffusing element, 2) anisotropy and 3) "impurities", i.e. elements of low concentration and not intentionally added.

Small atoms such as H, Fe, Ni up to O and N diffuse interstitially at a rate 10 to 20 times higher than that of larger atoms (Zr, Hf, Nb and Sn) that diffuse in substitutional manner.

The diffusion rate is anisotropic in the α-Zr lattice. The interstitial diffusion rate is three times larger along the c- compared to that in the a-axis while the substitutional diffusion rate is only slightly larger along the c-axis compared to that along the a-axis, *Hood, 1988, Ref. 5*.

"Impurities" may impact the substitutional diffusion rate. It has been shown that e.g., the Hf diffusion rate in α-Zr was two orders of magnitude larger in Zr with 50 ppm of Fe compared to that in Zr with < 1 ppm of Fe, *Hood, 1988, Ref. 5*.

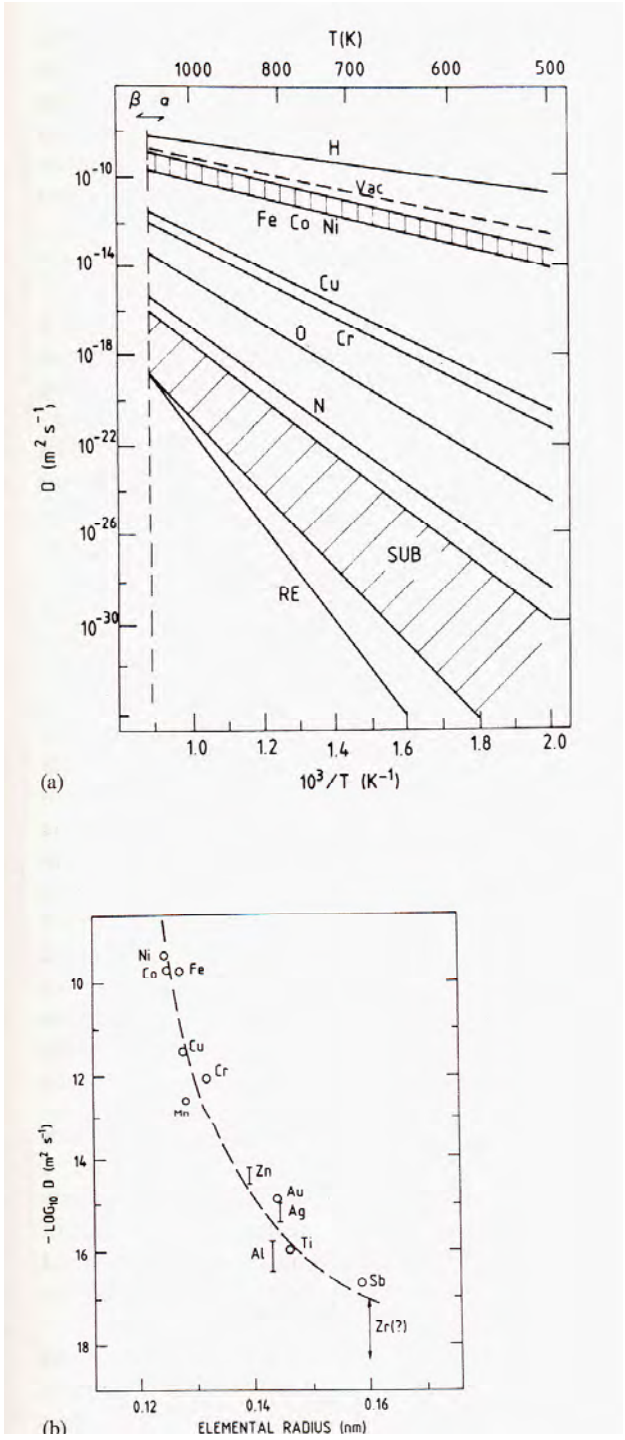

Figure 3-1: (a) Self and solute diffusion data in α-Zr. (b) Correlation between pre-exponential factor for diffusion in α-Zr and atom size, *Hood, 1988, Ref. 5.*

4 ALLOYING ELEMENTS IN ZIRCONIUM ALLOYS

4.1 OXYGEN

Oxygen was initially considered as an impurity but later was regarded as an alloying element. It is added in the form of ZrO_2 powder to the compacts before melting. The normal range is about 800 to 1600 wtppm and the effect of the oxygen addition is to increase the material strength, specifically the yield strength, by solution strengthening. Too high oxygen content will make the material brittle and therefore difficult to manufacture. The Zr-O phase diagram is shown in Figure 4-1. During high-temperature oxidation such as during a LOCA[1], a layer of oxygen stabilised α-zirconium is formed between the beta-quenched structure and the zirconium oxide. This α-zirconium layer is very brittle due to its high oxygen concentration.

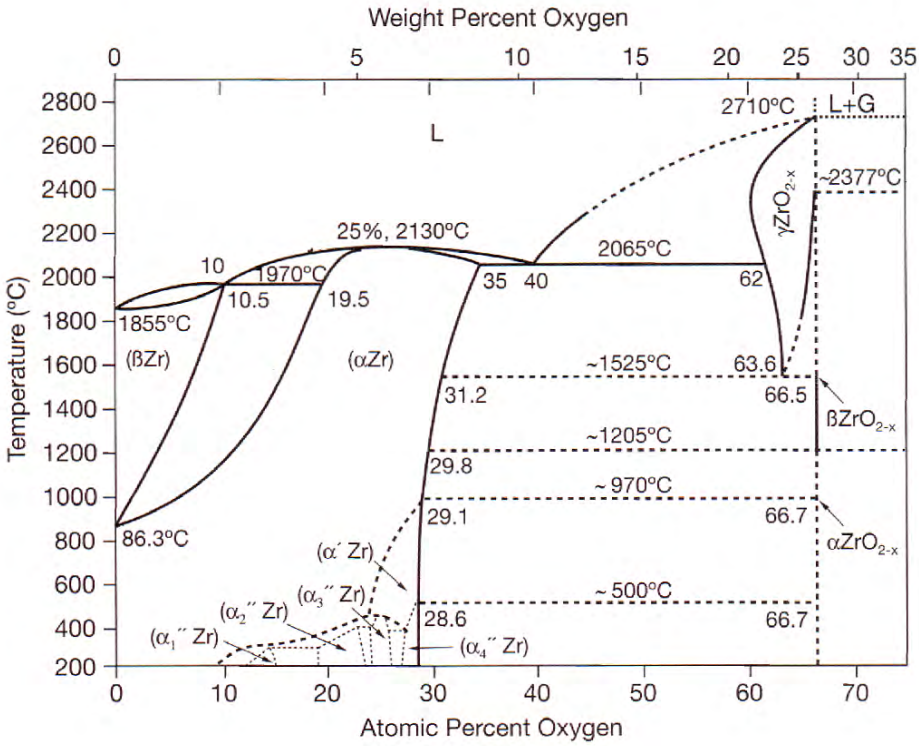

Figure 4-1: Zr-O phase diagram, *Abriata, 1986, Ref. 6.*

[1] *Loss of Coolant Accident*

4.2 HYDROGEN

Hydrogen is not an alloying element and the ASTM specification limits the hydrogen content to 25 ppm. However, during irradiation hydrogen is picked up to some extent by the material through the waterside corrosion. Hydrogen atoms are located at tetrahedral sites in the Zr h.c.p. lattice up to the solubility limit (about 15 ppm at 200°C and 200 ppm at 400°C), *Lemaignan and Motta, 1994, Ref. 1*. Above the solubility limit, hydrogen precipitates as the equilibrium δ f.c.c. phase, $ZrH_{1.66}$, Figure 4-2. Pure zirconium hydride therefore contains 18200 wtppm hydrogen. Metastable b.c.c. γ hydride, ZrH, will precipitate out, if the cooling rate is high, *Weatherly, 1981, Ref. 7*. Due to the volume expansion induced by the precipitation of the hydrides, this new phase tends to reduce its strain energy by nucleating on specific crystallographic planes. Habit planes are $\{10\bar{1}0\}$ for pure Zr and $\{10\bar{1}7\}$ for Zircaloys, in epitaxy with the matrix according to the relationship $(111)_\delta \| (0001)_{Zr}$, *Lemaignan and Motta, 1994, Ref. 1*. The subsequent growth of the hydrides occurs in the plane subjected to maximum tensile stresses or in the basal plane if unstressed, *Kearns and Woods, 1966, Ref. 8*. Thus, the texture of the material and also its stress state are crucial parameters to control the hydride precipitation.

Hydrides in zirconium alloys may have significant impact on material performance in-reactor, such as corrosion rate, dimensional stability, creep, secondary degradation of failed fuel and ductility during normal operation, during transients and accident conditions.

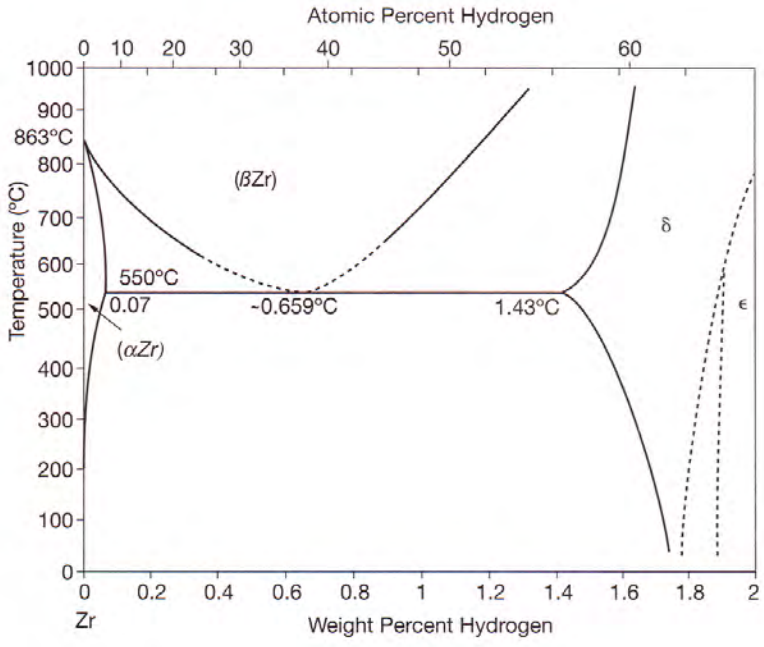

Figure 4-2: Zr-H phase diagram, *Zuzek et al., 1990, Ref. 9*.

4.3 CARBON

Carbon was another impurity that turned into an alloying element. At high temperatures carbon is soluble in α-Zr up to about 100 wtppm and only sparingly soluble in β-Zr. It forms a very stable precipitate, zirconium carbide, upon which the β- and α-Zr phases nucleate upon heating and cooling, respectively. The existence of zirconium carbides appears to promote the *basket weave* structure instead of the *parallel plate* morphology, Figure 4-3.

The *parallel plate* structure is undesirable since it reduces material ductility during subsequent plastic deformation as explained in the sequel. Normally, the different grains in a material have different crystallographic orientations. Transgranular[2] cracks propagate along specific crystallograhic planes and each time the crack intersects a grain boundary, the crack needs to be re-directed in the new grain (with another orientation) so it can propagate along the same preferred crystallographic plane as in the previous grain. However, there is a significant activation energy for re-directing the crack. Consequently, the necessary number of re-directions of the crack will decrease with increasing grain size which in turn will make the material more prone to cracking, i.e., less ductility. It is well-known that ductility decreases with increasing grain size. In the *parallel plate* structure, all the α-Zr grains, nucleated within the previous β-grain, have the same crystallographic orientation. This situation will facilitate crack propagation since the crack may propagate through the whole previous β-grain, before it needs to be redirected.

Carbon in solution also seems to increase the strength of the material. The ASTM specification limits the carbon content to 270 wtppm.

[2] *Cracks can either be intergranular, i.e., propagate along the grain boundaries or transgranular, i.e., propagate along specific crystallographic planes within the grain.*

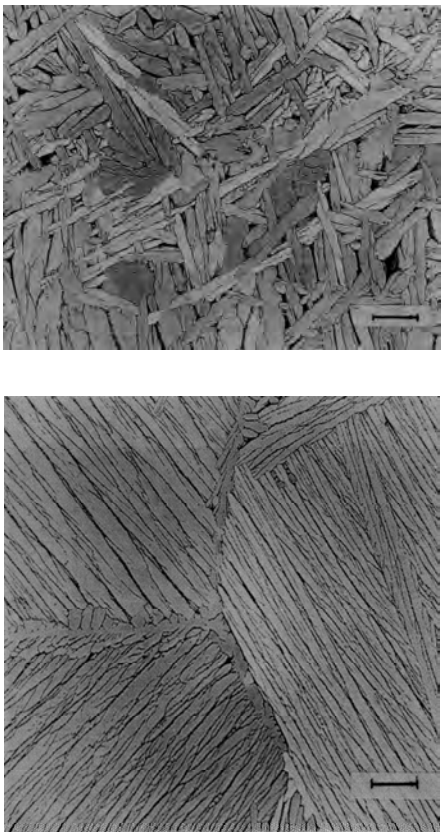

Figure 4-3: "Basket weave" (top) and "parallel plate" (bottom) structure of Zircaloy (scale mark indicates 50 μm), *Charquet and Alheritiere, 1987, Ref. 10*.

4.4 OTHER ELEMENTS IN SMALL CONCENTRATIONS

Silicon may also be considered today as an alloying element. It shows a limited solubility in the α- and β-Zr phases and appears to nucleate the α and β-Zr phases during beta heat treatments, Figure 4-4, therefore influencing the propensity for basketweave structure formation during quenching. It seems that silicon forming zirconium silicides promote nucleation of second phase particles upon cooling from the β-Zr phase, thus making the second phase particles overall smaller in size.

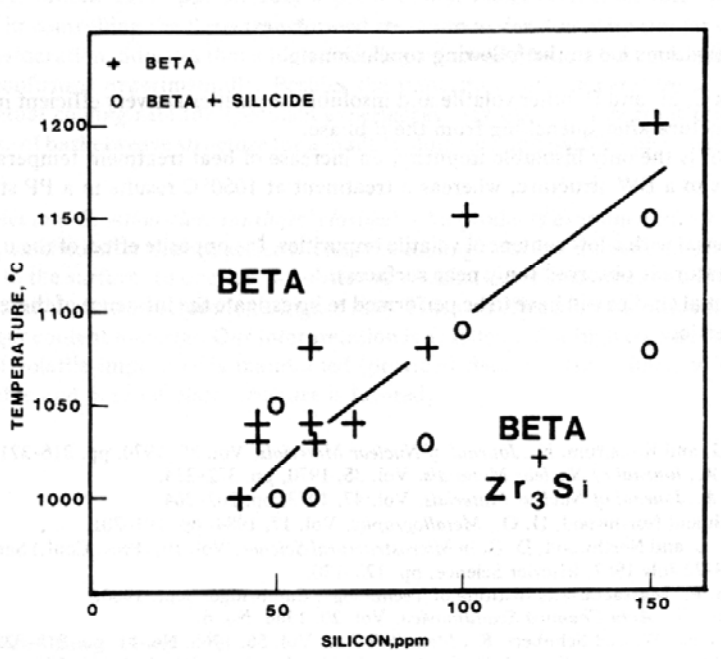

Figure 4-4: Transus beta/beta+silicide in Zircaloy, *Charquet and Alheritiere, 1987, Ref. 10.*

Chlorine combines with zirconium to form chlorides which are virtually insoluble in the beta phase and appears as filaments or stringers after deformation. As shown in Figure 4-5, for chlorine contents above the solubility limit of 1 to 2 ppm, the chlorides promote the form of *basket weave* structure when the metal is cooled rapidly from the beta phase field. The *basket weave* structure is a result of nucleation of the beta -> alpha transformation by the chloride particles.

In addition, other impurities may also impact the beta-quenched microstrucure, Table 4-1.

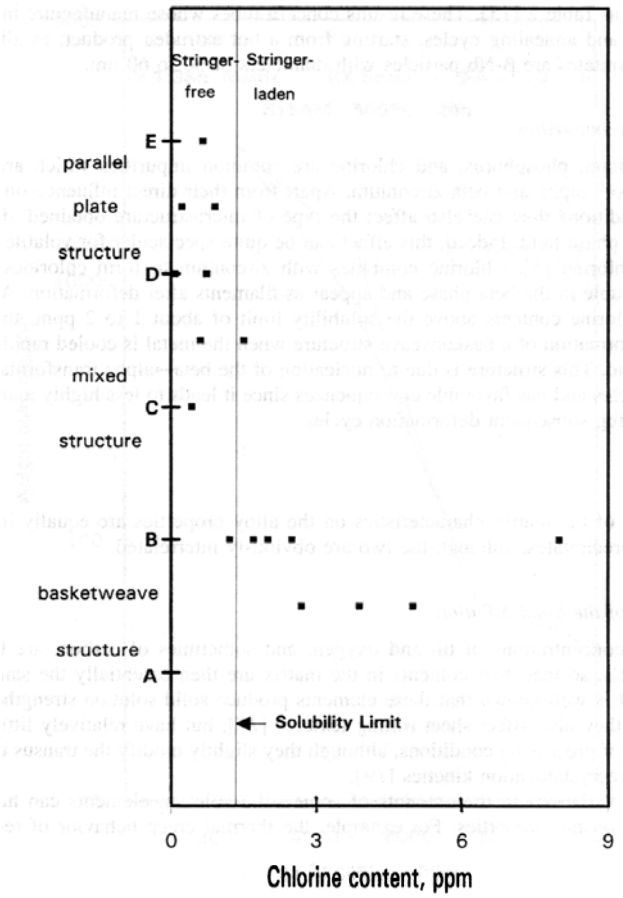

Figure 4-5: Influence of chlorine content on the beta heat treated microstructure, *Charquet, 2000, Ref. 11.*

Table 4-1: Effect of impurities on the microstructure of 50 g Zircaloy buttons (BW=basket weave structure, PP=parallel plate structure), Charquet and Alheritiere, 1987, Ref. 10.

Added Element, ppm	As	Microstructure	
		As-Melted	After β Quench from 1050°C
None	...	PP	PP
Na = 14	NaOH	PP	PP
Na = 16	NaCl	BW and PP	BW and PP
K = 33	KOH	PP	PP
K = 21	KCl	BW and PP	BW and PP
Ca = 21	CaO	PP	PP
Ca = 18	$CaCl_2$	BW and PP	BW and PP
Mg = 18	MgO	PP	PP
Mg = 17	$MgCl_2$	BW and PP	BW and PP
Si = 60	Si metal	PP	PP
Si = 130	Si metal	PP	PP
C = 100	carbon black	BW and PP	BW and PP
C = 200	carbon black	BW and PP	BW and PP

4.5 TIN

Tin is an alloying element and was initially added to mitigate the detrimental effect of nitrogen, picked up by the material during manufacturing, on corrosion performance. Later work has also shown that Sn additions also increases the material strength, specifically the creep resistance. The phase diagram is shown in Figure 4-6.

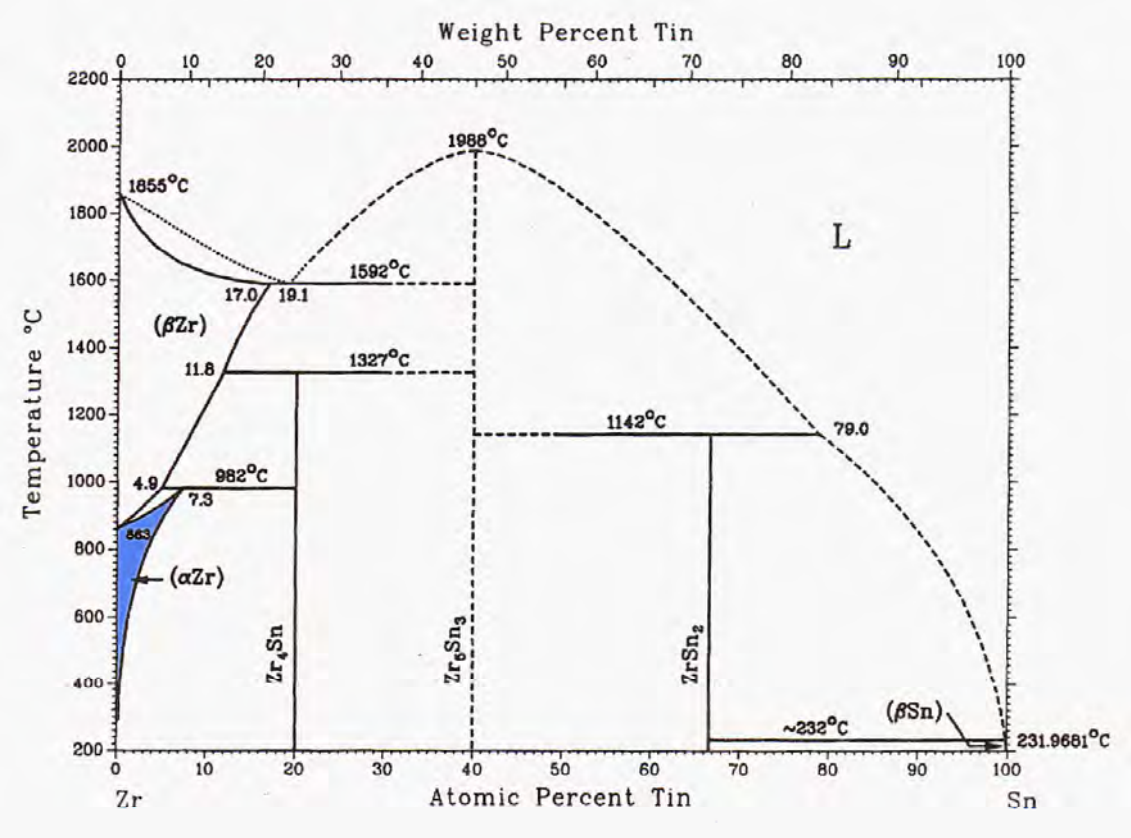

Figure 4-6: Zr-Sn phase diagram, *TECDOC 996, 1998, Ref. 12*.

4.6 IRON, NICKEL AND CHROMIUM

Iron, Chromium and Nickel dramatically improves corrosion resistance in zirconium. All these elements are completely dissolved in the β phase at Zry-2 and –4 compositions but have very low solubility in the α zirconium phase, Figure 4-7, Figure 4-8, and Figure 4-9.

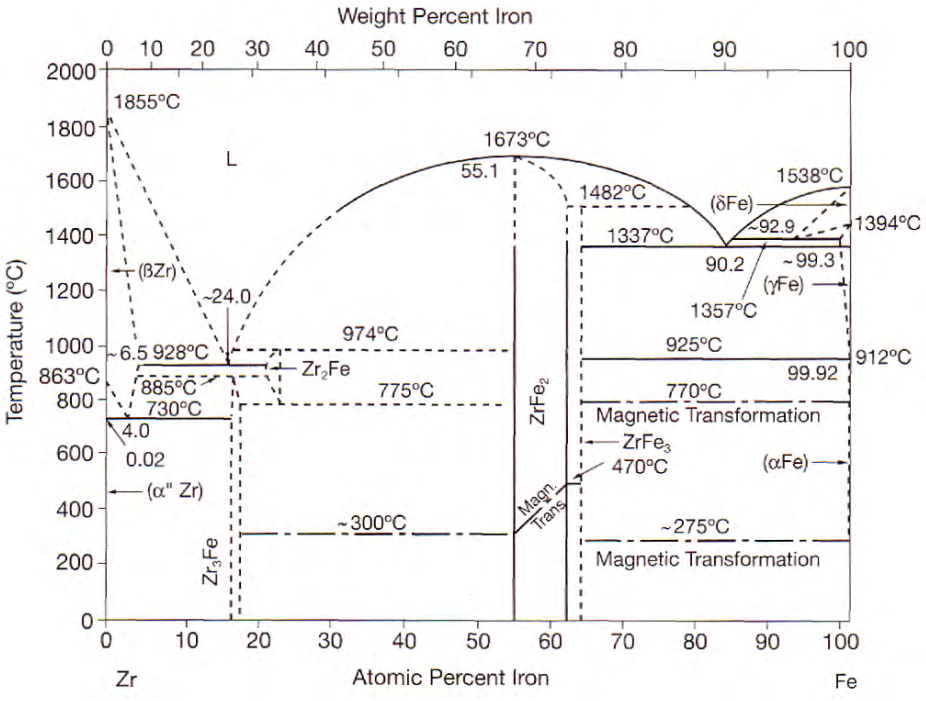

Figure 4-7: Zr-Fe phase diagram, *Arias et al., 1988, Ref. 13.*

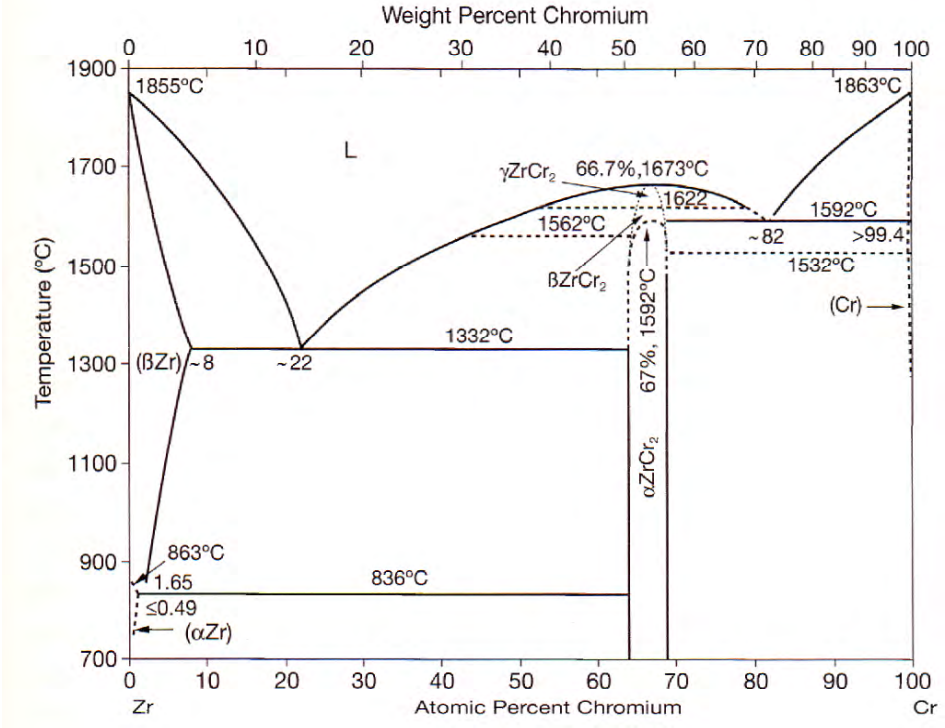

Figure 4-8: Zr-Cr phase diagram, *Arias and Abriata, 1986, Ref. 14.*

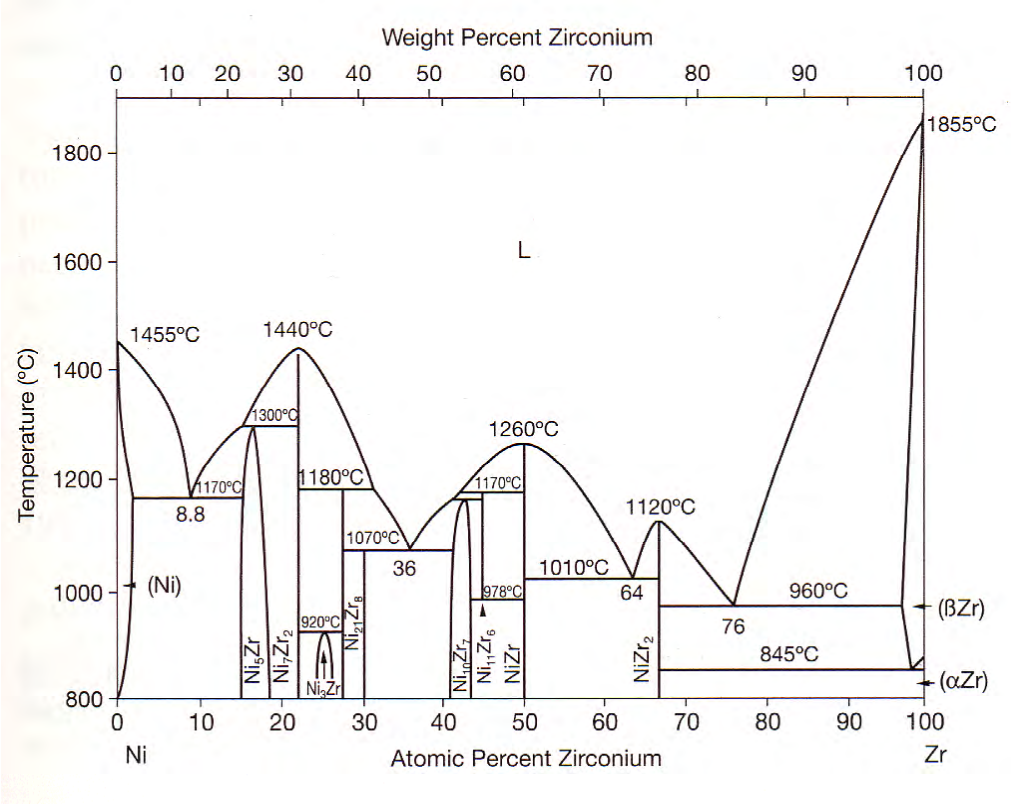

Figure 4-9: Zr-Ni phase diagram, *Nash an Jayanth, 1994, Ref. 15*.

4.6.1 Solubility

The solubility of Fe and Cr in zirconium was determined to 120 and 200 ppm at maximum solubility temperature, respectively, and Figure 4-10 and Figure 4-11. The maximum solubility of Fe+Cr was in the same investigation assessed to about 150 ppm at 800°C, Figure 4-12.

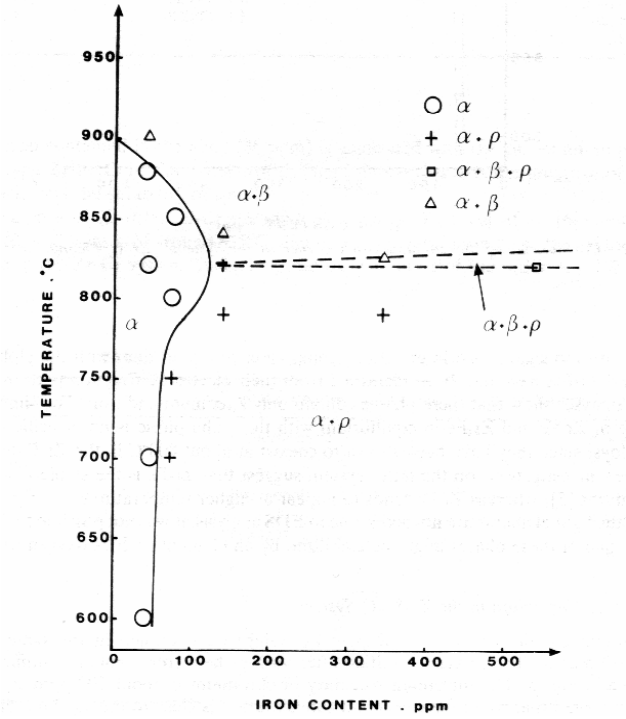

Figure 4-10: Zirconium-rich corner of the system: Zr (1.4%Sn0.1%O)-Fe, *Charquet et al., 1989, Ref. 16.*

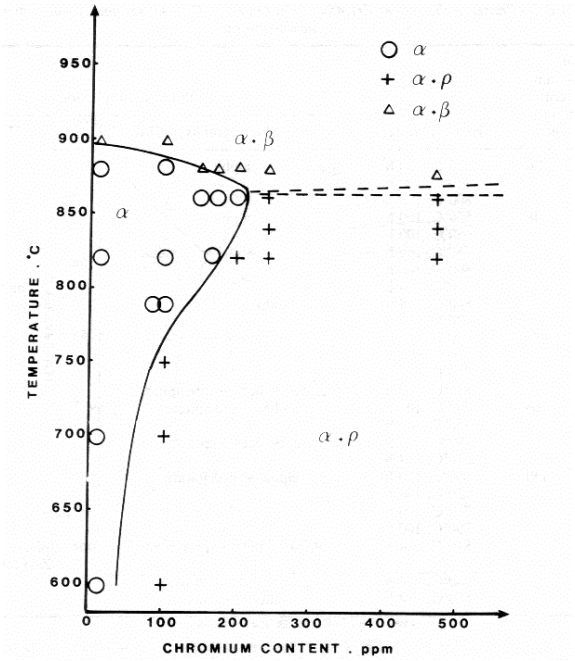

Figure 4-11: Zirconium-rich corner of the system: Zr(1.4%Sn0.1%O0.0036Fe)Cr, *Charquet et al., 1989, Ref. 16.*

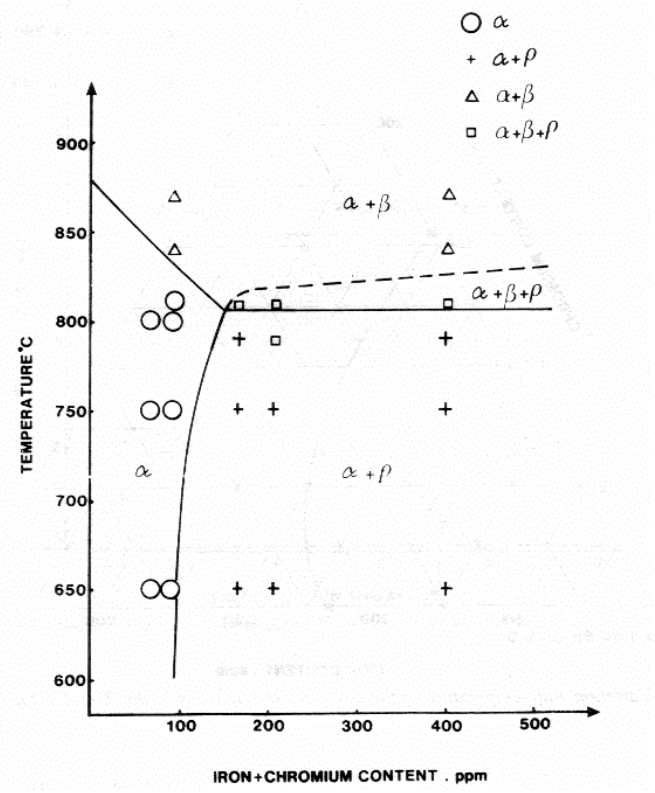

Figure 4-12: Zirconium-rich corner of the system: Zr(1.4%Sn0.01%O)-Fe + Cr, *Charquet et al., 1989, Ref. 16*.

Direct measurements of the zirconium matrix composition in Zry-4 PWR cladding tubes by atom probe analysis, indicated Fe and Cr contents in the matrix ranging from 110 to 220 and 90 to 140 wtppm, respectively, *Wadman et al., 1993, Ref. 17*. The same investigation revealed that directly after beta-quenching at 20°C/sec. from 1080°C the Fe and Cr concentration was 230 and 270 wtppm, respectively in the Zry-4 matrix. After an additional anneal at 1 h at 565°C of the beta-quenched material, the corresponding concentrations had dropped to 140 (Fe) and 130 (Cr) wtppm. The authors stated that the reason that a supersaturated matrix of Fe and Cr could not be maintained in the beta-quenched material was due to the high diffusion rates of Fe and Cr at high α temperatures. In these conducted experiments the matrix solubility of a Zry-2 material heat treated in the same way as that of the studied Zry-4 PWR material was found to be 190, 70 and 180 wtppm of Fe, Cr and Ni, respectively. Similar studies reported by *Kruger, et al., 1992, Ref. 18*, reported 33, 48 and 50 wtppm solubilities for Fe, Cr and Ni, respectively, with the absolute values changing depending on the exact heat treatment history. It is clear that accurate solubility numbers are difficult to determine but that the solubility of reactor operating temperatures of these elements is on the order of 100 wtppm.

4.6.2 Second phase particles

Garzarolli et al., 1996, Ref. 19, examined the main characteristics of Zr-Sn-Fe-Cr alloys with up 1.7 %Sn, up to 1%Fe and Cr, up to 120 ppm Si, and up to 50 ppm, *Table 4-2*. He reported that in alloys with Fe/Cr ratio < 4, almost all second phase particles are of the $ZrCr_2$ or $Zr(Fe,Cr)_2$ type but that sometimes other types of Fe containing precipitates with little or no Cr can be seen. The authors state that other precipitates often also contain some Si or Ni (always existing as an impurity if not added) to form $Zr_2(Fe,Ni)$ or $Zr_2(Fe,Si)$. The size of the $Zr_2(Fe,Si)$, which is observed at Si contents above 50 to 80 ppm, is normally very small and crystal structure examinations indicate that it is based upon Zr_2Si, *Garzarolli et al., 1996, Ref. 19*. The authors further argues that if the Fe/Cr ratio is > 4, Zr_3Fe is formed in addition to the Laves phase $Zr(Fe,Cr)_2$.

Table 4-2: Characteristics of second phase particle according to literature and Siemens results, Garzarolli et al., 1996, Ref. 19.

Type	Remark	Melting or Decomposition Temperature	Crystal Structure (a and c in nm)	Growth Rate (relative)
$Zr(Fe,Cr)_2$	most frequent SPP in Zry-4, Fe/Cr = 0 to 4		in $\alpha+\beta$-range: fcc, $a = 0.71$ in α:hex, $a = 0.5$, $c = 0.83$	medium
$ZrCr_2$		1620°C	>950°C: fcc, $a = 0.72$ else: hex, $a = 0.51$, $c = 0.83$	slow
$ZrFe_2$		1675°C	fcc, $a = 0.71$	
$Zr_2(Fe,Ni)$	appears sometimes		bct, $c = 0.65$, $a = 0.55$	medium-fast
Zr_2Ni		1150°C	bct, $c = 0.66$, $a = 0.53$	
Zr_2Fe		974°C	bct, $c = 0.64$, $a = 0.54$	
$Zr_2(Fe,Si)$	appears if Si > 50–80 ppm		bct, $c = 0.66$, $a = 0.53$	very slow
Zr_2Si		2110°C	bct, $c = 0.66$, $a = 0.53$	
Zr_3Fe	appears if Fe/Cr > 4	885°C	orthorhombic, $a = 0.33$, $b = 1.1$, $c = 0.88$	very fast
Zr_3Si	formed in the β-range		tetr, $a = 1.1$, $c = 0.55$	

Garzarolli et al., 1996, Ref. 19, also studied the growth characteristics of different precipitate types in several Zr-Sn-Fe-Cr heats with the same Fe/Cr ratio. Type A material represented Zr-Sn-Fe-Cr heats with a very low Si content while type B material had a larger Si content of 60 to 100 ppm and a slightly lower *A*-parameter[3]. i.e., heat input during manufacturing after the last beta-quenching. Figure 4-13 shows that material A has a mono-modal distribution and only $Zr(Fe,Cr)_2$ second phase particles. On the other hand, material B has a bi-modal intermetallic distribution with a high number density of very small $Zr_2(Fe,Si)$ second phase particles and about the same number density and size distribution of $Zr(Fe,Cr)_2$ second phase particles as that of material A. The growth characteristics of the different intermetallics are shown in Figure 4-14. At comparable temperature/time histories, Zr_3Fe are the largest intermetallics, larger than that of $Zr(Fe,Cr)_2$ precipitates that in turn are larger than that of $ZrCr_2$and $Zr_2(Fe,Si)$ precipitates. *Garzarolli et al., 1996, Ref. 19*, could show that the second phase particle size was correlated to the homologous process temperature, i.e., the process temperature related to the respective melting or decomposition temperature of the different intermetallics, Figure 4-15.

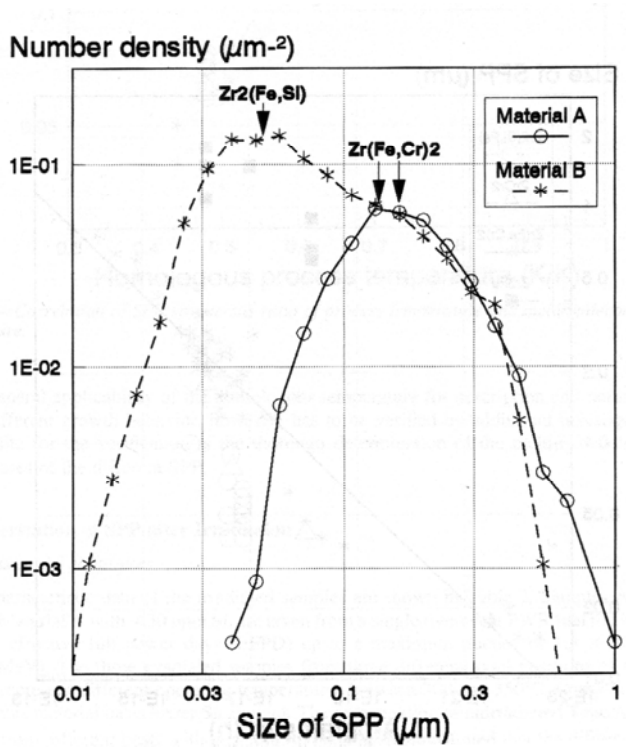

Figure 4-13: Size distribution of second phase particle in materials A (very low Si content) and B (Si content varying between 60 to 100 ppm), *Garzarolli et al., 1996, Ref. 19*.

[3] *The concept of A-parameter is described in detail in Appendix B*

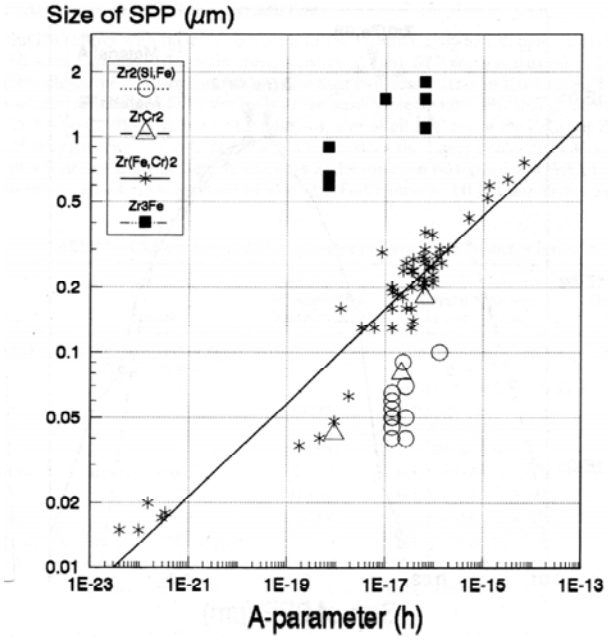

Figure 4-14: Correlation between A-parameter (the value of Q/R is 40000K) and second phase particle size, *Garzarolli et al., 1996, Ref. 19*.

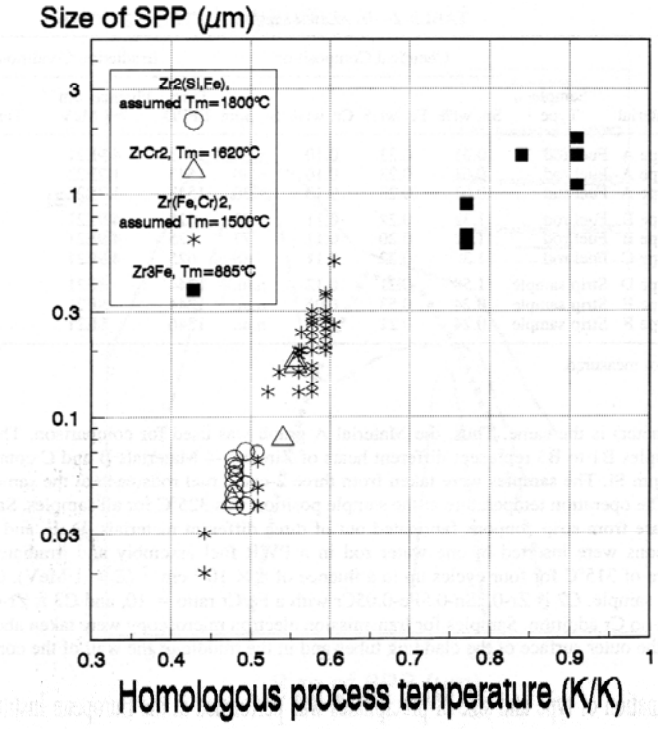

Figure 4-15: Correlation of second phase particle size versus ratio of process temperature and melting/decomposition temperature, *Garzarolli et al., 1996, Ref. 19*.

Since no Ni is added to Zry-4 only the $Zr(Cr,Fe)_2$ intermetallic is normallly found in this alloy. However, in Zry-2 where Ni has been added both $Zr(Cr,Fe)_2$ and $Zr_2(Ni,Fe)$ types of precipitates are found, Figure 4-16. The $Zr(Cr,Fe)_2$ particle is essentially a $ZrCr_2$ particle where some of the Cr has been replaced by Fe. Correspondingly the $Zr_2(Ni,Fe)$ precipitate is a Zr_2Ni precipitate where Ni is replaced by Fe.

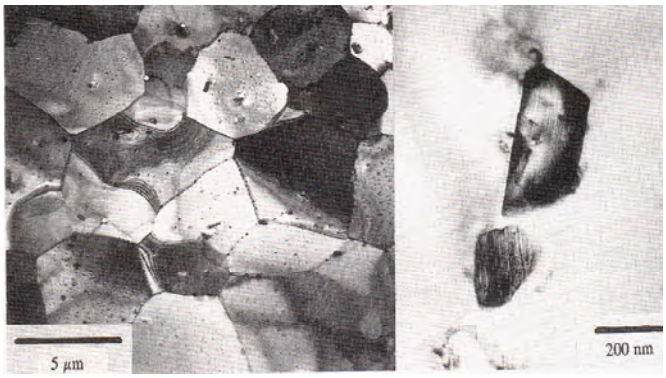

Figure 4-16: Typical distribution of second phase particle $Zr(Cr,Fe)_2$ and $Zr_2(Ni,Fe)$ in recrystallised Zircaloy-2, *Lemaignan and Motta, 1994, Ref. 1*.

The actual chemical composition in the second phase particle depends on alloy chemistry and manufacturing process. The impact of these parameters were studied in Zry-4 by *Charquet, 2000, Ref. 11*. He found that the Fe/Cr ratio in the precipitates were very close to that in the alloy but that as the cooling rate increased from the β-region, the Fe/Cr ratio in the $Zr(Cr,Fe)_2$ precipitates was less than that in the alloy, Figure 4-17.

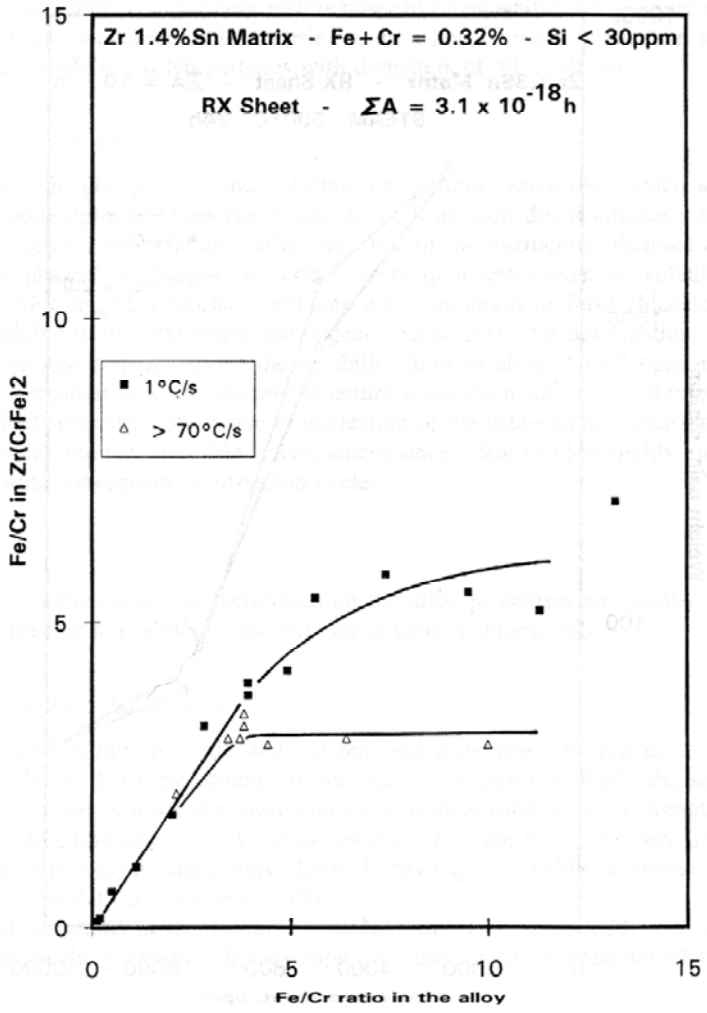

Figure 4-17: Influence of alloy chemistry and cooling rate after intermediate beta annealing on the composition of $Zr(Cr,Fe)_2$ precipitates, *Charquet, 2000, Ref. 11*.

During manufacturing the vendor tries to get an optimum second phase particle size distribution in the Zircaloys to get good corrosion performance in reactor.

There are three important parameters relative to the second phase particles to keep in mind to get good corrosion performance of Zircaloys: 1) the second phase particle size distribution, 2) the second phase particle chemical composition and/or structure and, 3) how homogeneous the precipitates are distributed in the material.

Normally, smaller precipitates are required to get good corrosion performance in BWRs compared to that to get good corrosion resistance in PWR environments. However, if the precipitates become too small in a BWR, accelerated corrosion may occur. The second phase particles must initially be somewhat larger than the necessary size to hinder accelerated corrosion since the particles tend to dissolve during irradiation in a BWR. The dissolution tendency increases as precipitates become smaller in size. Also the particle chemical composition and/or structure will impact the precipitate dissolution tendency. In PWRs the second phase particle dissolution tendency is much smaller due to the higher irradiation temperature in a PWR that will make the precipitates more stable.

It has also been shown that these precipitates must be uniformly distributed in the material to get good corrosion performance. Actually, the reason for the failure of Zry-3 in the early developments of Zircaloy was due to inhomogeneous distribution of precipitates, stringers, in the material that resulted in poor corrosion performance. If the second phase particles are uniformly distributed in the Zry-3 material, the material corrosion performance is excellent. The Siemens duplex ELS alloy targeted for high corrosion duty PWR plants is a modification of Zry-3. However, since the mechanical strength is too low in a Zry-3 type material due to its low Sn content, Siemens has solved this problem by adding a thin corrosion resistant layer of this Zry-3 type material at the clad outer diameter onto the core of Zry-4. This concept is named Duplex.

4.7 NIOBIUM

Scientists in the former Soviet Union pioneered the use of niobium as the prime alloying element to get good corrosion and mechanical performance of the zirconium material.

Nb is completely soluble in the β zirconium phase, Figure 4-18. A monotectoid transformation occurs at about 620°C and at about 18.5 at% Nb.

Lemaignan and Motta, 1994, *Ref. 1*, mention that by water quenching from the β or the upper α+β phase, the former β grains will transform by a martensitic phase transformation into a α' martensite supersaturated h.c.p. phase with Nb. However, if the cooling rate from the β phase is slow or if the quenched structure is annealed at temperatures below the monotectoid transformation temperature, the α' is transformed into: 1) β precipitating at the lath and at twin boundaries within the lath as well as 2) α. According to *Jovanovic et al, 1996, Ref. 21*, further annealing involves in most cases the precipitation of the metastable ω-phase and β_{Zr}-phase (≈20 wt% Nb) as an intermediate step in the β-phase decomposition into α (<0.6 wt% Nb) and β_{Nb} (≈85 wt% Nb), Figure 4-19:

$$\beta \rightarrow \omega + \beta_{Zr} \rightarrow \alpha + \omega + \beta_{Zr} \rightarrow \alpha + \beta_{Zr} \rightarrow \alpha + \beta_{Zr} + \beta_{Nb} \rightarrow \alpha + \beta_{Nb}$$

It has been shown that β_{Zr} results in poor corrosion performance while the existence of β_{Nb} improves the corrosion performance in Zr-Nb alloys.

Thus to ensure that a finished product of Zr-Nb material does not contain any β_{Zr}, it is important to either: 1) keep the annealing temperatures below the monotectoid transformation temperature during the late stage of manufacturing or 2) perform the final , below the monotectoid transformation, at such a long time that all metastable β_{Zr} has decomposed into α and β_{Nb}.

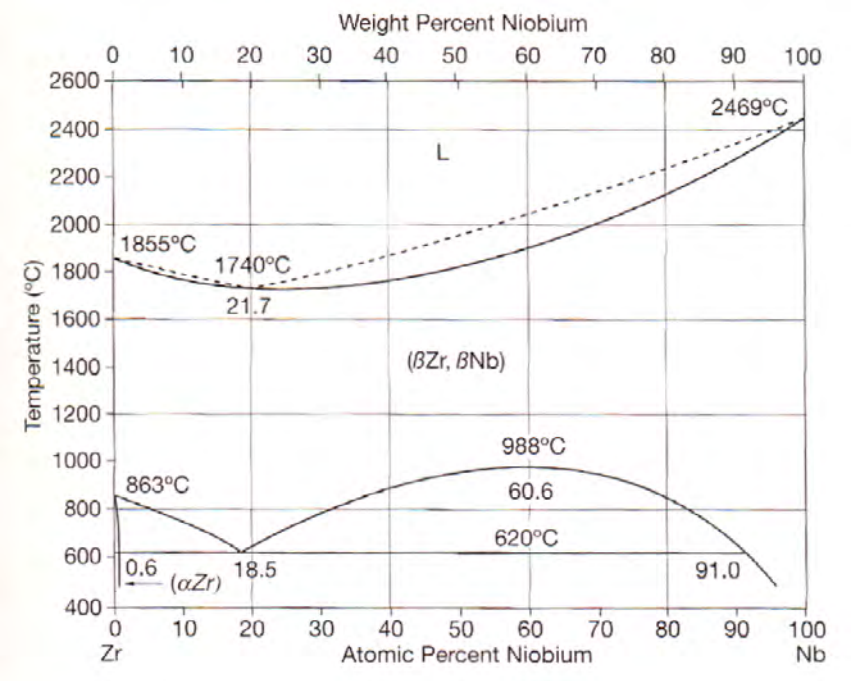

Figure 4-18: Zr-Nb phase diagram, *Abriata and Bolcich*, 1982, *Ref. 20*.

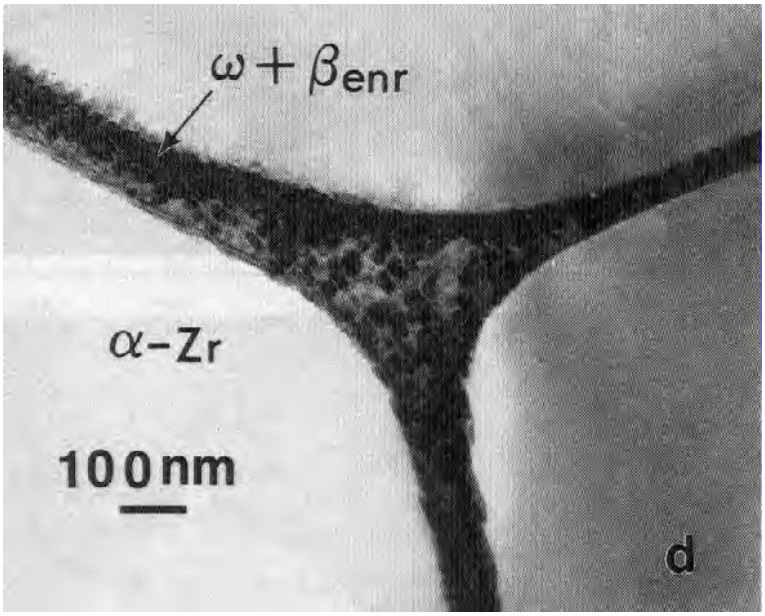

Figure 4-19: Alloy microstructure of Zr1Nb after corrosion testing at 573 K, β_{enr} is equivalent to β_{Zr}, *Urbanic et al., 1994, Ref. 22*.

5 FABRICATION OF LWR CLADDING TUBES, SHEET AND PLATE

Nearly all the zirconium metal is extracted from zircon sand, Zr-Hf SiO_4, occurring in beach sand all over the world. The zirconium to hafnium ratio in zircon is about 50 and since Hf has a very large thermal neutron cross section, it is crucial that as much Hf as possible is separated from zirconium during the manufacturing process.

Despite the fact that zirconium is one of the most common elements in earth crust, the metal cost is about the same as that of silver. The reason for this unexpected high cost is related to the great affinity that zirconium has for oxygen that makes processing complicated. The manufacturing process of different light water reactor, LWR, zirconium alloy products may be divided into three steps: 1) production of Zr-sponge, 2) ingot manufacturing and, 3) final product fabrication.

5.1 ZR-SPONGE MANUFACTURING

An outline of the Zr sponge fabrication is shown in Figure 5-1.

The first step is to convert zircon into $ZrCl_4$, through a carbo-chlorination process performed in a fluidised bed at 1200°C according to the reaction, Lemaignan and Motta, 1994, *Ref. 1*:

$$ZrO_2(+SiO_2 + HfO_2) + 2C + 2Cl_2 \rightarrow ZrCl_4(+SiCl_4 + HfCl_4) + 2CO$$

After this step, Zr and Hf are separated by one of the following processes, according to the same authors:

Wet chemical process– after reaction with ammonium thiocyanate, SCN NH_4, a solution of hafnyl-zirconyl-thiocyanate, $(Zr/Hf)O(SCN)_2$ is obtained. A liquid-liquid extraction is performed with methyl-isobutyl-ketone and finally a Hf-free $ZrCl_4$ is obtained. A calcine process then converts the chloride to ZrO_2 and a second carbo-chlorination produces $ZrCl_2$.

Extractive distillation process - within a mixture of KCl-$AlCl_3$ as solvent at 350°C. The vapour phase, generated by a boiler at the lower part of the distillation column, is enriched in Hf, while the liquid phase traps the Zr.

After one of the two above processes, Zr metal is obtained by the Kroll process in which gaseous $ZrCl_4$ is reduced by liquid magnesium at 850°C in an oxygen-free environment. Any Mg remnants are subsequently removed from the sponge cake by distillation at 1000°C. The sponge cake is then fractured and the pieces are carefully inspected where contaminated pieces showing up as discoloration are discarded.

High purity Zr can be obtained by another process, the Van Arkel process in which Zr reacts with iodine at moderate temperature, gaseous phase transport as ZrI_4 and decomposition of the iodide at high temperature on an electrically heated filament. This process is considerably more expensive than the Kroll process.

Table 5-1 compares the purity of Zr-sponge produced by the Kroll process and Zr crystal bar by the Van Arkel process.

5 FABRICATION OF LWR CLADDING TUBES, SHEET AND PLATE

Nearly all the zirconium metal is extracted from zircon sand, Zr-Hf SiO_4, occurring in beach sand all over the world. The zirconium to hafnium ratio in zircon is about 50 and since Hf has a very large thermal neutron cross section, it is crucial that as much Hf as possible is separated from zirconium during the manufacturing process.

Despite the fact that zirconium is one of the most common elements in earth crust, the metal cost is about the same as that of silver. The reason for this unexpected high cost is related to the great affinity that zirconium has for oxygen that makes processing complicated. The manufacturing process of different light water reactor, LWR, zirconium alloy products may be divided into three steps: 1) production of Zr-sponge, 2) ingot manufacturing and, 3) final product fabrication.

5.1 ZR-SPONGE MANUFACTURING

An outline of the Zr sponge fabrication is shown in Figure 5-1.

The first step is to convert zircon into $ZrCl_4$, through a carbo-chlorination process performed in a fluidised bed at 1200°C according to the reaction, Lemaignan and Motta, 1994, *Ref. 1*:

$$ZrO_2(+SiO_2 + HfO_2) + 2C + 2Cl_2 \rightarrow ZrCl_4(+SiCl_4 + HfCl_4) + 2CO$$

After this step, Zr and Hf are separated by one of the following processes, according to the same authors:

Wet chemical process– after reaction with ammonium thiocyanate, SCN NH_4, a solution of hafnyl-zirconyl-thiocyanate, $(Zr/Hf)O(SCN)_2$ is obtained. A liquid-liquid extraction is performed with methyl-isobutyl-ketone and finally a Hf-free $ZrCl_4$ is obtained. A calcine process then converts the chloride to ZrO_2 and a second carbo-chlorination produces $ZrCl_2$.

Extractive distillation process - within a mixture of KCl-$AlCl_3$ as solvent at 350°C. The vapour phase, generated by a boiler at the lower part of the distillation column, is enriched in Hf, while the liquid phase traps the Zr.

After one of the two above processes, Zr metal is obtained by the Kroll process in which gaseous $ZrCl_4$ is reduced by liquid magnesium at 850°C in an oxygen-free environment. Any Mg remnants are subsequently removed from the sponge cake by distillation at 1000°C. The sponge cake is then fractured and the pieces are carefully inspected where contaminated pieces showing up as discoloration are discarded.

High purity Zr can be obtained by another process, the Van Arkel process in which Zr reacts with iodine at moderate temperature, gaseous phase transport as ZrI_4 and decomposition of the iodide at high temperature on an electrically heated filament. This process is considerably more expensive than the Kroll process.

Table 5-1 compares the purity of Zr-sponge produced by the Kroll process and Zr crystal bar by the Van Arkel process.

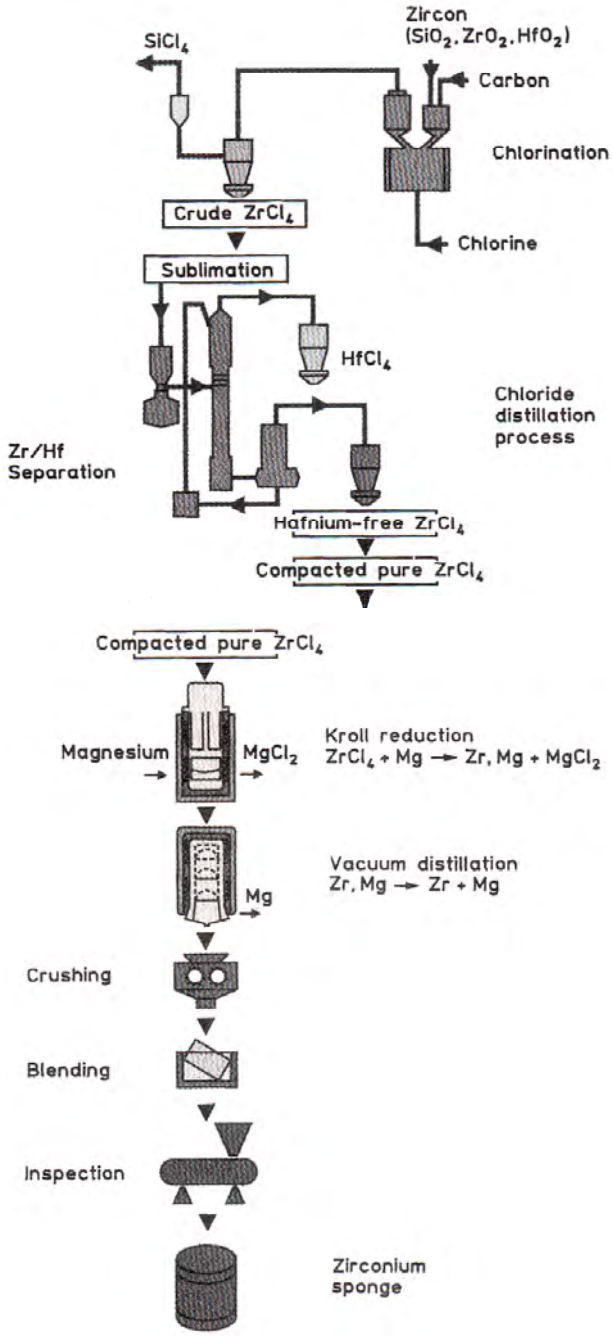

Figure 5-1: One typical process for sponge manufacturing, *Lemaignan and Motta, 1994, Ref. 1.*

Table 5-1: Impurity levels of high-purity Zr sponge and Crystal bar (Zr-X-Bar) used (units in ppm), Isobe et al. 1996, Ref. 23.

Element	Zr-X-Bar[2]	EB-Zr[1,2]	Zr Sponge
Fe	6	2	~950
Cr	3	<0.01	65
Al	2	<0.01	25
Ti	<0.1	0.05	25
Si	0.2	30	40
Cu	0.1	0.02	5
W	<0.1	0.2	25
Hf	26	80	75
Mg	<0.1	<0.01	—
O	70	600	1100
C	25	90	110
N	<10	30	45

[1] EB-Zr: refined from sponge zirconium by EB-melting.
[2] Analyzed by GDMS.

5.2 INGOT MANUFACTURING

An outline of the ingot manufacturing is shown in Figure 5-2.

Zirconium sponge, recycle material from earlier manufacturing, and alloying elements are put together into an electrode. Normally, sponge-based briquettes and solid recycle material are assembled and welded either by electron beam in vacuum or plasma arc welding in argon atmosphere into an ingot typically between 50 to 80 cm in diameter weighing from 3 to 8 tons, Figure 5-3.

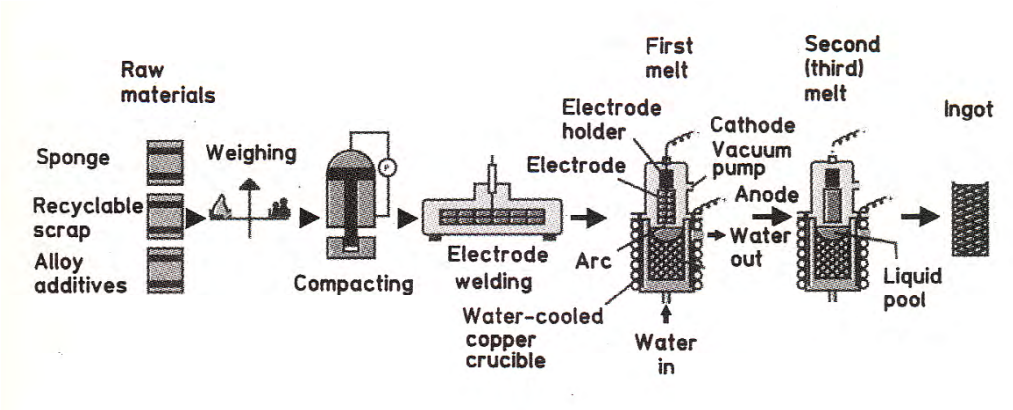

Figure 5-2: Ingot manufacturing, Lemaignan and Motta, 1994, Ref. 1.

6 SPECIFICATION, TESTING AND INSPECTIONS

The different zirconium alloy products are manufactured according to specifications, specific for each fuel vendor. These specifications generally follow the generic format of the American Society for Testing and Materials, ASTM, standards. These ASTM standard includes the following technical points.

6.1 COMPOSITION

The samples are taken from the ingot at 3 to 5 different elevations and the ingot analysis forms a part of the product certificate. Hydrogen, oxygen and to some extent nitrogen can be absorbed by the zirconium alloy product during processing and specifications require that a sample for hydrogen, oxygen and nitrogen analysis is taken from the finished tubing.

6.2 MECHANICAL PROPERTIES

Tensile testing, usually at room temperature and at some elevated temperature near 370°C are done according to ASTM standards to assess yield and ultimate tensile strength and ductility.

Internally pressurized burst tests are sometimes used to assess mechanical properties where the resulting circumferential elongation is measured.

6.3 CORROSION RESISTANCE

A test in 400°C, 1500 psi steam during 72 hours, ASTM Method G2, is used to assess uniform corrosion performance. The acceptance criterion is a maximum oxide weight gain of 22 mg/dm^2 and a visual examination of the oxide film. In this test one can e.g. identify fluoride contamination from the pickling process showing up as whitish spots in the otherwise black oxide.

Also for BWR applications a steam corrosion test, not yet standardised by ASTM, at 500 to 520°C for about 24 hours is used to check material susceptibility for nodular corrosion.

6.4 HYDRIDE ORIENTATION

The hydride orientation is crucial for the in-pile ductility of the cladding tube material. The maximum hydrogen content in the final product is 25 ppm much less than the solubility limit at operation temperature, about 100 wtppm. However, since hydrogen is absorbed by the zirconium material during the corrosion reaction with water/steam in the reactor, the hydrogen content can be increased to levels higher than the solubility limit late in life. The bulk hydride orientation is very much related to the material texture. At the tube surface, the orientation is influenced by any residual stresses introduced during fabrication or straightening.

A test has been developed to assess what the hydride distribution would look like in-reactor at higher hydrogen concentrations than the solubility limit of the finished cladding tube. This method involves charging the cladding tube specimen with about 200 ppm of hydrogen and subsequent metallographic examinations. Hydride platelets with angles smaller than a specific value, normally about 40° to the radial direction, are classified as radial and the other as circumferential hydrides. The ratio of radial to the total number of platelets is the hydride fraction, f_n. It is normally specified that $f_n < 0.3$.

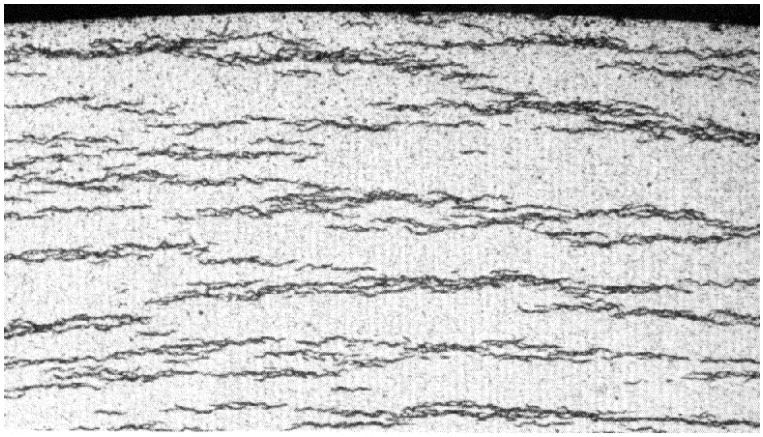

Figure 6-1: Micrograph of typical SANDVIK tubing showing circumferential hydrides, Schemel, 1989, Ref. 24.

6.5 MICROSTRUCTURE

There is generally a vendor-specific requirement on grain size. Grain size measurements can only be done on RXA materials. Grain size is often expressed as an "ASTM number", where the number is inversely related to an average grain diameter. A typical Zircaloy grain size is ASTM 12, which is an average grain size of 6 microns.

6.6 DIMENSIONS

Minimum and maximum values are given for the inside and outside diameters and length. Maximum are specified for ovality, bow and squareness of the end cut. A minimum is specified for wall thickness. Ultrasonic testing is used for diameter and wall thickness determination.

6.7 ULTRASONIC TESTING, UT

Ultrasonic testing, UT, is used to assure freedom from unacceptable flaws. A maximum size of a reference notch is specified. This test involves using small artificial defects of the same size (typically 0.0015 inch deep, 0.004 inch wide and 0.062 inch long) but various orientations: one oriented axially addition, one circumferentially, on each at the cladding inner and outer surfaces. Any tube that returns a signal equal to or larger than that returned by the standard notch is rejected.

It is important to keep in mind that this mehod does not measure the flaw depth but rather the projected area of the notch.

6.8 CRYSTAL ORIENTATION, TEXTURE

Contractile Strain Ratio, CSR, is a mechanical test to assess the texture in the material. It consists of carefully measuring the diameter of the tube at different locations and measuring the distance between a series of scribe marks along the tube. The tube is then plastically strained in tension and the measurements are repeated. The changes in diameter and length makes it possible to determine the ratio of circumferential strain to wall thickness strain which is the CSR value. A value less than one indicate a circumferential texture and values larger than two a radial texture. See Section 5.3.1 for a discussion of texture. Fuel suppliers have an internal texture specification which is strictly adhered to. The normal texture for tubing as expressed by the Kearns texture parameters are on the order of

f_r (radial) = 0.60

f_a (axial) = 0.07

f_n (through thickness) = 0.33

6.9 SAMPLING FREQUENCY

Composition, except for gases, is based on the analysis of the ingot. Dimensional and UT flaw testing is done in a continuous scan of each tube and other tests are generally done on two random samples from each lot of material.

6.10 TEST METHODS

Most testing is done according to ASTM or American national Standards Institute, ANSI, standards or their counterpart in non-US countries.

6.11 VISUAL INSPECTION

This inspection is visual by the unaided eye under strong ligthing. The tubes are examined for flaws at the outer and inner surface.

7 DETAILED FABRICATION OF CERTAIN ZIRCONIUM ALLOYS

In this section detailed information found in the open literature of commercial zirconium alloys are presented.

7.1 ZR-NB ALLOYS

7.1.1 Pressure tubes for CANDU reactors

Table 7-1 shows typical chemical composition of pressure tubes and an outline of the Zr2.5Nb pressure tube fabrication is shown in *Figure 7-1*.

Urbanic and Griffith, 2000, Ref. 39, reported on the Zr2.5Nb pressure tube manufacturing, as follows. The CANDU pressure tubes are formed by extrusion at about 815°C. They are then cold-drawn about 27 % to give a final tube of 6.3 m with a final tube thickness of 4.3 mm and an inside diameter of about 104 mm. The final tube contains both <*a*> - and <*c*>-type dislocations and with a dual-phase α/β structure. The alpha-phase grains are platelets containing about 0.6 to 1wt% Nb in solution. The α-grains are stacked together and separated by a non-equilibrium β-phase containing about 20 wt% Nb. A final autoclaving results in partial decomposition of the β-phase with the formation of Nb-depleted ω precipitates in a Nb-enriched matrix (up to about 50 wt%; the average composition in the β-phase remains about 20 wt%. A typical microstructure is shown in *Figure 7-2*.

Table 7-1: Chemical specification for CANDU Zr2.5Nb pressure tubes fabricated before 1987, Davies and Shewfelt, 2000, Ref. 40.

Element	Specification (up to 1987)
Niobium	2.4–2.8 wt%
Oxygen	900–1300 ppm[a]
Carbon	<270 ppm
Chlorine	...
Chromium	≤200 ppm
Hydrogen	≤25 ppm[b]
Iron	≤1500 ppm
Nickel	≤70 ppm
Nitrogen	≤65 ppm
Phosphorus	...
Silicon	≤120 ppm
Tantalum	≤200 ppm
Zirconium and other impurities	Balance

[a] ppm by weight.
[b] 20-ppm hydrogen for ingot, 25-ppm hydrogen for final tube.

Since 1987, new data, Theaker et al., 1994, on fracture toughness has resulted in a modification of Table 7-1. The changes are: C, 125 ppm max; Cl, 0.5 ppm max; P, 10 ppm max; 0, 1000-1300 ppm; H, 5 ppm max.

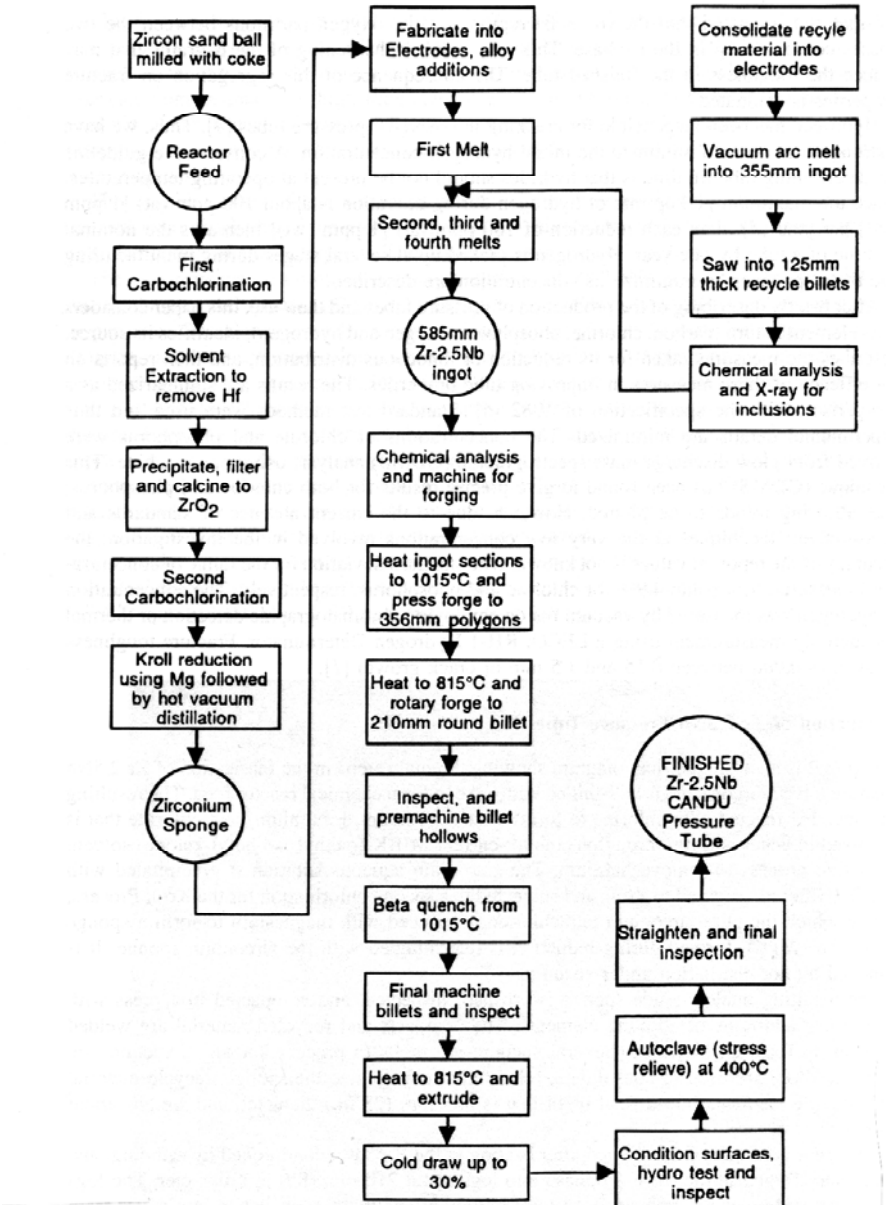

***Figure 7-1: Abridged flow chart for the fabrication of CANDU Zr2.5Nb pressure tubes,* Theaker et al., 1994, Ref. 41.**

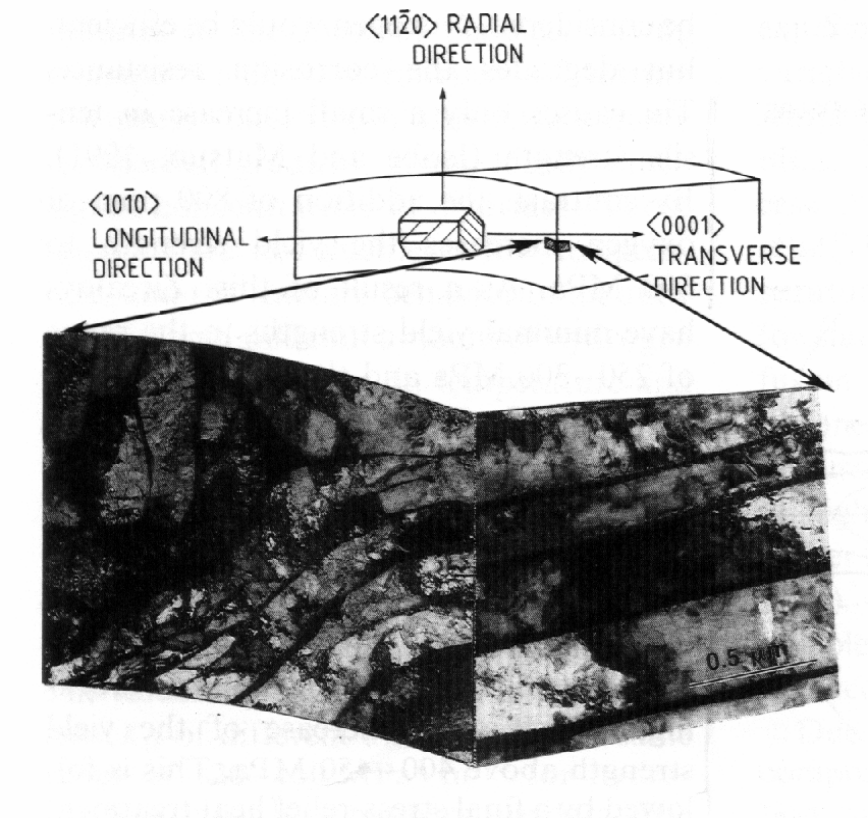

***Figure 7-2: Typical microstructure of Zr-2.5Nb pressure tubes: a layered structure of α Zr and β (Nb-Zr),* Lemaignan and Motta, 1994, Ref. 1.**

7.1.2 Materials for Russian WWER and RBMK Reactors

In the following *Nikulina et al., 1996, Ref. 42*, summarised the different Zr-Nb materials used for the Russian nuclear reactors. The alloy E635 is now recommended as a material for fuel claddings, guide tubes and spacer grids for WWER reactors to replace the E110 alloy to increase burnup. The alloy E635 is also intended to replace the Zr2.5Nb pressure tube material in RBMK reactors. The alloy E635 is used in RXA condition, except for pressure tubes when the alloy is used in SRA condition. The E110 alloy has been successfully used as fuel cladding material in WWER and RBMK reactors. The Zr used in E110 is a mixture of electrolytic and iodide Zr. The major fabrication steps of both E110 and E635 are the following:

1. Vacuum-arc furnace melting of a 1.2-ton ingot from a mixture of an electrolytic powder and iodide zirconium bars in the ratio ≈ 70:30,
2. β-forging (1070 to 900°C)
3. Water quenching of forged billets from the temperature of heating in the β-region (≈ 1050°C)
4. α-pressing (600 to 650°),
5. cold rolling in four or five stages with intermediate α-anneals (560 to 620°C)
6. Final recrystallization anneal in the α-region (560 to 620°C)

8 EFFECT OF FABRICATION-RELATED ATTRIBUTES ON IN-REACTOR PERFORMANCE

The previous chapters described various metallurgical and physical aspects of fabrication of zirconium alloys. Numerous interactions that affected fabricability were outlined. In this section, we will discuss how fabrication variables can affect in-reactor performance. A full description including effects from very low burnup to very high burnup is not attempted here, but will be the focus of a later report.

Table 8-1 reproduces a figure from a recent report on factors observed to affect fuel reliability, *Harbottle and Kennard, 2000, Ref. 49.* A few fabrication related factors are listed there. A more detailed listing of fabrication-related attributes related to specific fuel performance issues is given in *Table 8-2*. Some of the more important connections are described below.

Table 8-1 Factors in recent "failure" events affecting fuel reliability

Failure Mechanism or Event	Fuel Vendor(s) Affected	Plants Affected	Contributory Factors			
			Design	Testing	Fab, QA/QC	Operation
Grid-Rod Fretting	A	>8	X	X		
	A	2			X	
	B	>2			X	
	C	Various	X	X	X	
	D	>4	X		X	
Loss of DNB Margin	A	Various	X	X		
Primary Hydriding	B	Various			X	
Debris Filter Fretting	E	Various	X	X		
PCI (Primary)	F	Various	X	X		
PCI (Secondary)	Various	Various	X	X		
Axial Offset Anomaly	A, C	Various	X			X
Clad Collapse	A, C	2			X	
IFBA Helium Release	A	Various		X		
End Plug Piping	A	Various			X	
Cladding Flaws, Missing Pellet Surface	F	Various			X	
Incomplete Control Rod Insertion	A, G, H	Various	X	X		
End Plug Weld Defects	A	1			X	
	C	1			X	
	F	Various			X	
	I	1			X	
Debris Fretting	All	Various	X			X
Accelerated Corrosion	C	1	X			X
	Various	Various	X	X		

Table 8-2 Effect of fabrication-related attributes on in-reactor performance at medium to high burnup. No effect = 0; postulated effect = X; small effect = XX; large effect = XXX; uncertain = ?

										Corrosion			
Fabrication attributes	Hydride effects	Strength	Ductility	Toughness	Degradation	PCI	Creep	Growth	(hydride-related) Dimensions	Uniform	Nodular	Crud	Shadow
Texture	XXX	XXX	XXX	XXX	XX	XX	XXX	XXX	0	XX	XX	0	?
hydride orientation	XXX	XX	XXX	XXX	XX	0	0	0	0	XX	0	0	0
Final ht-treat - RX/SRA	XX	XX	XX	XX	XX	0	XXX	XXX	0	XX	0	0	?
SPP													
size	0	XX	XX	0	X	0	0	X	XX	XXX	XXX	XXX	XXX
distribution	0	0	XX	XX	XX	0	XX	0	XX	XXX	XXX	XX	?
chemistry	0	XX	XX	0	0	0	0	XX	XX	XXX	XX	XX	?
Sigma A	0	XX	XX	0	X	0	X	X	XX	XXX	XXX	XXX	XXX
Chemistry													
impurities	0	XX	XXX	XXX	X	0	XXX	X	X	XX	XX	XX	XX
alloying	XX	XXX	XXX	XXX	X	0	XXX	XXX	XX	XXX	XXX	XXX	XXX
Surface finish	0	0	0	0	0	0	0	0	0	XXX	XXX	XXX	X
Grain size	X	X	X	X	0X	XX	X	X	0	X	0	0	?

8.1 BWR/PWR DIFFERENCES

Some fabrication-related attributes have different effects depending on details of the reactor system being used. Some differences in standard PWRs and BWRs are given in *Table 8-3*.

Because of adequate corrosion resistance in the BWR environment, Zircaloy-2 continues to be the choice for BWR cladding, spacers and (generally) channels. In the higher temperature PWRs, corrosion of Zircaloy-4 at modern high burnups is sufficiently severe to require a change to different zirconium alloys. In general the fabrication issues for these new alloys are not new or different, although metallurgical details may be unique.

Table 8-3 Differences in PWRs and BWRs which affect cladding behavior

	BWR	PWR
Material	Zircaloy-2, RX	Zircaloy-4, CWSR Zircaloy variations, CWSR Zr-Nb alloys, RX/CWSR
Reactor water	boiling (70 bar) high O2 (200 ppb) core H2, 20 ppb	non-boiling, nominally (155 bar) low O2 (<5 ppb) core H2 >2000 ppb
Water additives (possible)	Zn, Pt, Rh, H (200 ppb)	H, Li, NH4, B, K
Clad temperature, °C	288-320	300-370
Corrosion _temperature dependence _neutron enhancement _type	 small large nodular, uniform	 large medium uniform
Current burnup target, (bundle ave.) MWd/KgU	50	60
Peak fluence, n/cm2 (E>1MeV)	~12 x 1021	~15 x 1021

8.2 EFFECTS OF FINAL HEAT TREATMENT

Because of high water pressure to prevent boiling in the PWR (although it should be noted that some modern PWRs do get boiling in the upper fuel rod regions) higher strength is required in the PWR fuel cladding. Therefore cold worked/stress relieved (CWSR) cladding is most often used (an exception is M5 (Zr-1Nb), which is used in the recrystallized (RX) condition). Early in service, the strength difference is significant; however later in life, beyond a burnup of about 10 MWd/KgU, radiation hardening causes RX and CWSR material to have about the same strength. A more long lasting effect is the influence on irradiation growth and creep. Figure 8-1 illustrates that the steady state creep rate is significantly higher for CWSR material. Whether the cladding is Zircaloy-2 or –4 is insignificant. In addition, both the fluence dependence and rate of growth depend on the final heat treatment, as illustrated in Figure 8-2 for 70% cold work/stress relieved and 0% cold work recrystallized Zircaloy. Since the growth is roughly proportional to the amount of cold work, small amounts of residual cold work can have real effects on the growth.

APPENDIX A – DEVELOPMENT OF TEXTURE

The following is a summary of the excellent review on texture done by *Tenckhoff, 1988, Ref. 25.*

DEFORMATION MECHANISMS IN HCP METALS

The *c/a* axial ratio varies from metal to metal and can attain a value larger or smaller than that for ideal sphere packing, 1.633, Figure 9-1.

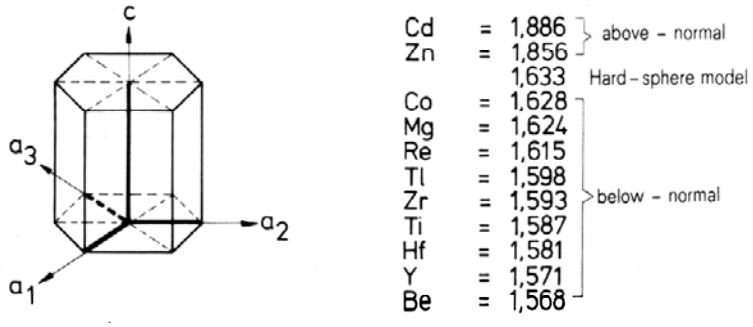

Figure 9-1: The *c/a* ratio for various hcp metals, Tenckhoff, 1988.

Plastic deformation at lower temperatures can be induced either by slip and/or by twinning.

Slip modes

There are two laws determining the slip behaviour of metals:

1) The slip system, slip plane and direction, that will first become active is the one with the largest difference between the resolved shear stress and the critical resolved shear stress. This is related to Schmid's law of resolved shear stress and discussed more in section A.1.3.
2) The slip plane and direction is normally the closed-packed plane and direction. This is related to that the Peierls-Nabarro forces are small for short Burgers vectors, i.e. in closed-packed directions, in planes with high atomic density.

The different possible slip systems are shown Figure 9-2. A slip system with a component in the *c* direction has been observed only under constraint and at high deformation temperatures according to Tenckhoff, 1988. However, irradiated materials are likely to be more prone to basal plane deformation, as shown by a change in deformation anisotropy. He further states that, apart from pyramidal slip modes, deformation with *c* components seems to occur primarily by twinning.

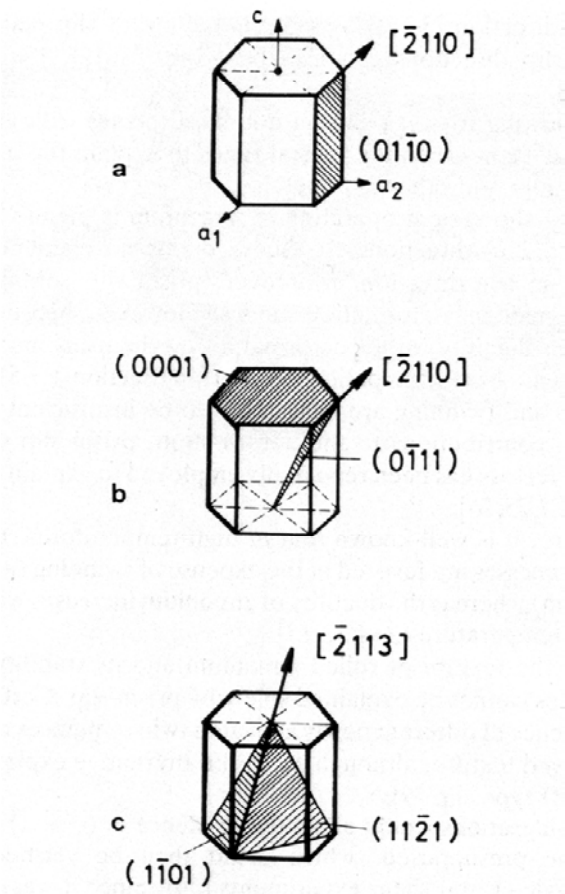

Figure 9-2: Slip systems in α-zirconium, Tenckhoff, 1988.

Twinning

The twinning process may be described by Figure 9-3. During twinning, the "northern half" of the reference sphere is deformed into a partial ellipsoid of the same volume. This is accompanied by homogeneous shear of the crystal lattice parallel to the equatorial plane such that the atom layers form mirror images of each other with respect to this plane. The shear associated with twinning leaves two lattice planes undistorted[6], K_1, and K_2, before twinning and K_2' after twinning. All crystal directions in the upper-left segment between K_1 and K_2 are shortened by the shear and all crystal directions to the right of this are extended. The undistorted planes K_1 and K_2 are normal to the shear plane and η_1 is the shear direction. The shear magnitude is defined as:

S=2cot 2Φ

[6] *This means that all distances and angles in these planes remain unchanged.*

The different twinning modes in zirconium are shown in Figure 9-4.

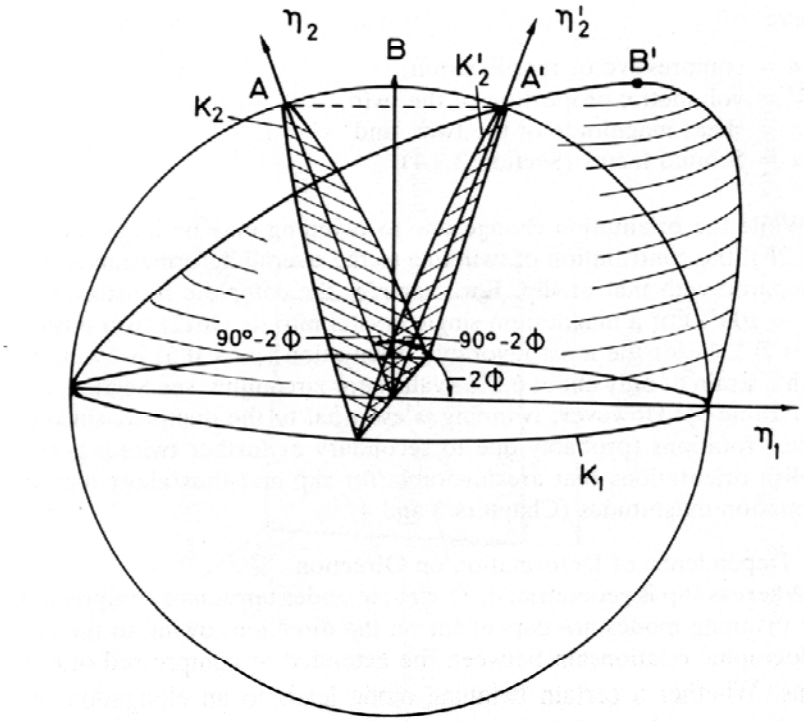

Figure 9-3: Relationship between reference sphere and twinning ellipsoid, Tenckhoff, 1988.

APPENDIX B – ANNEALING PARAMETER

To have a measure of the total heat input after the last beta-quenching the concept of an accumulated annealing parameter, *A*, has been proposed:

$$A = \Sigma t_i \exp\left(-Q / RT_i\right)$$

where

t_i is the time in hours at temperature T

Q is an activation energy

R is the gas constant and,

T_i is the temperature in Kelvin.

However, different activation energies have been used and the basis for the different activation energies are described more in the following.

MECHANICAL TESTS AND RECRYSTALLIZATION

Steinberg et al, 1984, Ref. 31, first introduced the expression annealing parameter based upon mechanical and recrystallization data of Zry-4.

He noted that the decrease of the yield strength, $R_{p0.2}$, with increasing annealing temperature followed an *S*-shaped curve, where the value $R_{p0.2}$ started from an upper plateau, $R_{p0.2}^{\max}$, followed by a step decrease, and ended in a second lower plateau, $R_{p0.2}^{\min}$, Figure 9-17. Rearranging the data from Figure 9-17, Figure 9-18 is obtained, where the slope of the lines, $a = Q/R$, is equal to 40 000 K.

In Figure 9-19 it is shown how the experimental results from Figure 9-18 are represented by just one straight line, when the following correlation is used:

$$\frac{R_{p0.2}^{\max} - R_{p0.2}}{R_{p0.2} - R_{p0.2}^{\min}} = k \bullet t \bullet \exp\left(-Q / RT\right) = kA$$

where *t* is the annealing time and *k* is a constant and the so called annealing parameter, *A*, is:

$$A = t \bullet \exp(-Q / RT)$$

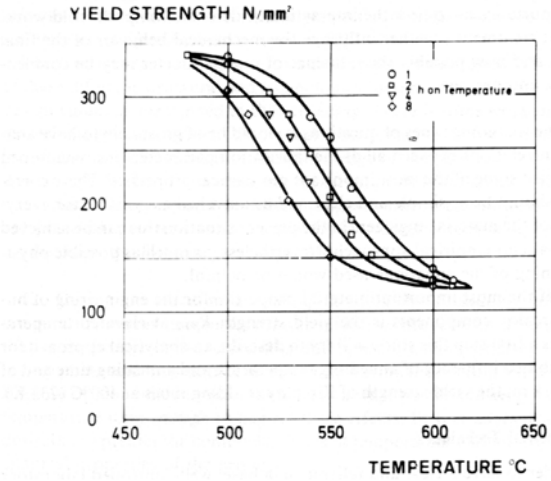

Figure 9-17: Dependence of the 400°C yield strength of Zry-4 cladding tubes on annealing temperature and time, Steinberg et al., 1984.

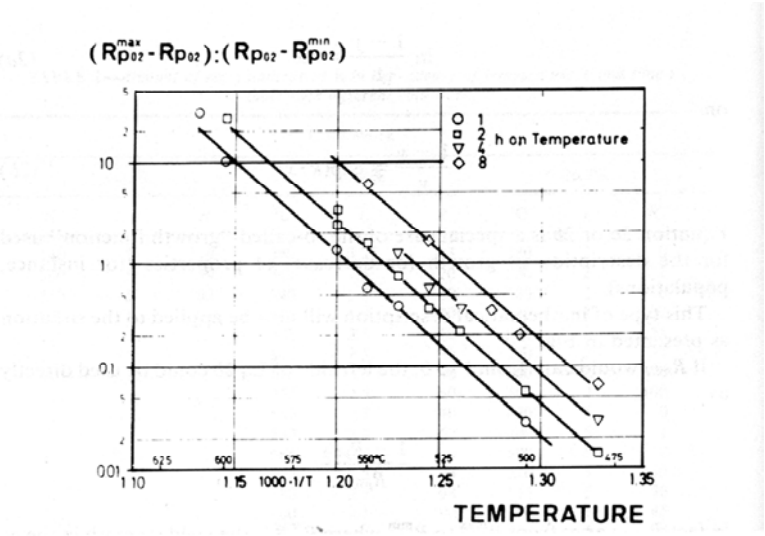

Figure 9-18: Correlation between yield strength and annealing temperature according to the function $\ln\left(R_{p0.2}^{\max} - R_{p0.2}\right) : \left(R_{p0.2} - R_{p0.2}^{\min}\right) = -a \bullet 1/T = \ln b$, Steinberg et al., 1984.

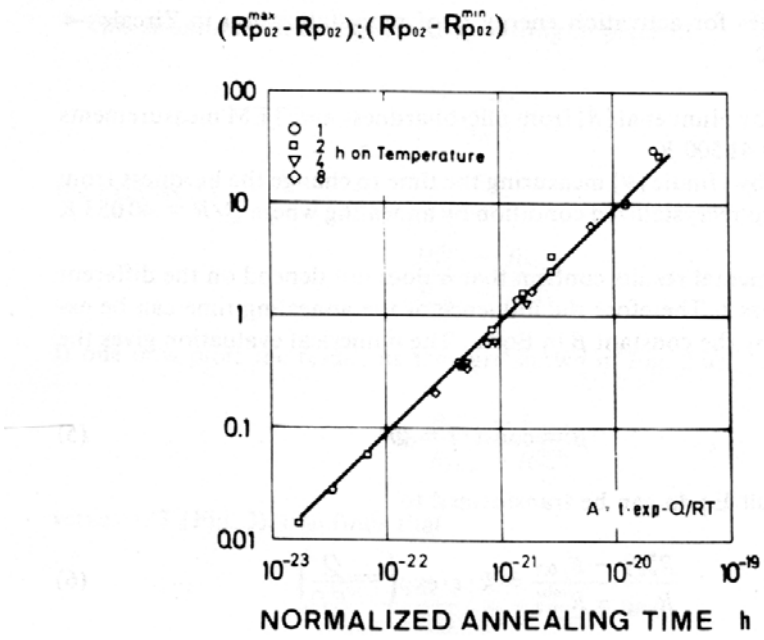

Figure 9-19: Correlation between annealing temperature and time expressed as $A = t \bullet \exp(-Q/RT)$ and the yield strength expressed as $\left(R_{p0.2}^{\max} - R_{p0.2}\right) : \left(R_{p0.2} - R_{p0.2}^{\min}\right)$, Steinberg et al., 1984.

In Figure 9-20 the experimentally found amount of recrystallisation, *R*, is plotted versus *A*, where *A* is defined as the fraction of area of recrystallised grains relative to the total area. The different amount of cold work is characterised by the parameter, ϕ. The slope of the line, corresponding to *–Q/R*, in Figure 9-21 is 40 000 K.

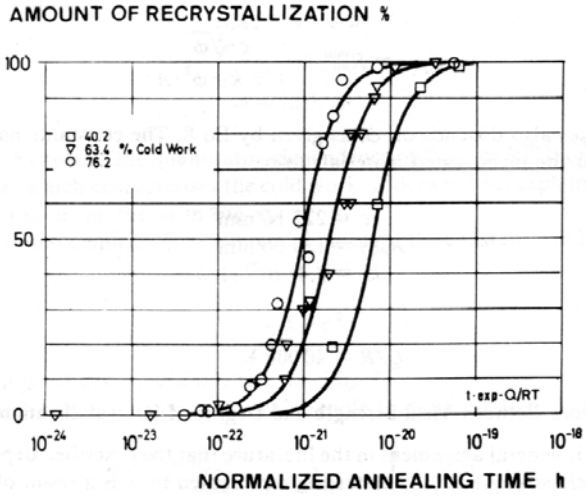

Figure 9-20: Dependance of recrystallisation on the annealing time A for various amounts of cold work, Steinberg et al., 1984.